AD-A150 938 CHARGE TRANSFER POLARIZATION AND RELAXATION EFFECTS IN THE AUGER LINESHAP..(U) GEORGE WASHINGTON UNIV WASHINGTON D C DEPT OF CHEMISTRY D E RAMAKER ET AL. 1/1

UNCLASSIFIED NOV 84 TR-15 N00014-80-K-0852 F/G 7/4 NL

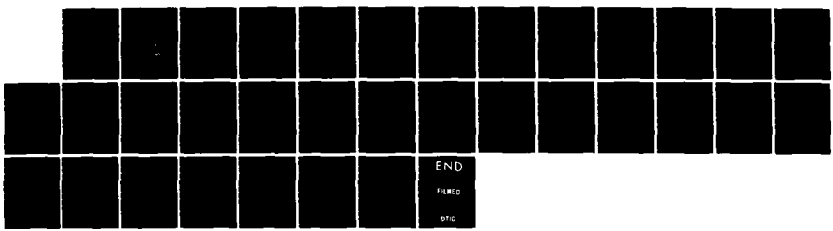

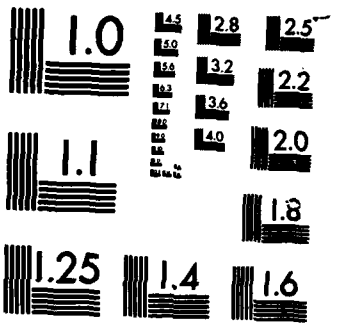

OFFICE OF NAVAL RESEARCH

N00014-80-K-0852

Task No. 056-681

Technical Report No. 15

CHARGE TRANSFER, POLARIZATION, AND RELAXATION EFFECTS IN THE AUGER LINESHAPES OF Si

By

David E. Ramaker, F. L. Hutson, N. A. Turner, and W. N. Mei

Prepared for Publication

in

Physical Review B

George Washington University
Department of Chemistry
Washington, D.C. 20052

November 1984

(2)

SECURITY CLASSIFICATION OF THIS PAGE (When Data Entered)

REPORT DOCUMENTATION PAGE	READ INSTRUCTIONS BEFORE COMPLETING FORM
1 REPORT NUMBER: No. 15	2 GOVT ACCESSION NO. / 3 RECIPIENT'S CATALOG NUMBER
4 TITLE (and Subtitle): CHARGE TRANSFER, POLARIZATION AND RELAXATION EFFECTS IN THE AUGER LINESHAPES OF Si.	5 TYPE OF REPORT & PERIOD COVERED: Technical Report / 6 PERFORMING ORG. REPORT NUMBER
7 AUTHOR(s): D. E. Ramaker, F. L. Hutson, N. H. Turner and W. N. Mei	8 CONTRACT OR GRANT NUMBER(s): N00014-80-K-0852
9 PERFORMING ORGANIZATION NAME AND ADDRESS: Chemistry Department, George Washington University, Washington, D.C. 20052	10 PROGRAM ELEMENT, PROJECT, TASK AREA & WORK UNIT NUMBERS: Prog. Elem. No. 61153N, Task Area No. PP 013-08-01, Work Unit # NR 056-681
11 CONTROLLING OFFICE NAME AND ADDRESS: Office of Naval Research, Dept. of Navy, 800 N. Quincy Street, Washington, D.C. 22217	12 REPORT DATE: Nov. 1984 / 13 NUMBER OF PAGES: 50
14 MONITORING AGENCY NAME & ADDRESS(if different from Controlling Office)	15 SECURITY CLASS. (of this report): Unclassified / 15a DECLASSIFICATION/DOWNGRADING SCHEDULE

16 DISTRIBUTION STATEMENT (of this Report)
This document has been approved for public release and sale; its distribution is unlimited.

17 DISTRIBUTION STATEMENT (of the abstract entered in Block 20, if different from Report)

18 SUPPLEMENTARY NOTES
Submitted for publication in Physical Review B

Cont'd

19 KEY WORDS (Continue on reverse side if necessary and identify by block number)
Auger electron spectroscopy, silicon, screening, shakeoff, charge polarization.

20 ABSTRACT (Continue on reverse side if necessary and identify by block number)
The Auger lineshapes of Si are quantitatively interpreted noting particularly the core hole screening effects as exhibited through charge transfer, polarization, and atomic relaxation. The KL_1V $KL_{23}V$ and $L_1L_{23}V$ lineshapes reflect a core hole screened DOS consistent with the core hole in the final state of these processes. A DOS appropriate for the screened core hole is obtained by distorting the theoretical DOS for the ground state utilizing the Green's function for a tight binding Hamiltonian and a central cell potential. The $L_{23}VV$ and KVV lineshapes reveal some distortion effects due to final state hole correlation,

DD FORM 1 JAN 73 1473 EDITION OF 1 NOV 65 IS OBSOLETE S/N 0102-014-6601 | Unclassified SECURITY CLASSIFICATION OF THIS PAGE (When Data Entered)

85

1 of 1

and large final state shakeoff effects arising from radial contraction of the 3s orbital on the atom with the initial core hole. The latter atomic relaxation effect is evident from the apparent lack of ss and sp contributions. The $KL_{23}L_{23}$ lineshape is interpreted in the context of similar lineshapes for Na, Mg, Al and P; all show plasmon losses, and except for P, initial state shakeoff contributions.

KLsub1V KLsub23V

Lsub1Lsub23V

CHARGE TRANSFER, POLARIZATION, AND RELAXATION EFFECTS ON THE AUGER LINESHAPES OF Si.

D. E. Ramaker, F. L. Hutson*, N. H. Turner+, W. N. Mei*

+Chemistry Division
Naval Research Laboratory
Washington, D.C. 20375

And

*Chemistry Department
George Washington University
Washington, D.C 20052

Lsub23VV

KLsub23Lsub23

Abstract

The Auger lineshapes of Si are quantitatively interpreted noting particularly the core hole screening effects as exhibited through charge transfer, polarization, and atomic relaxation. The KL_1V, $KL_{23}V$ and $L_1L_{23}V$ lineshapes reflect a core hole screened density of states, DOS, consistent with the core hole in the final state of these processes. A DOS appropriate for the screened core hole is obtained by distorting the theoretical DOS for the ground state utilizing the Green's function for a tight binding Hamiltonian and a central cell potential. Comparison of the $L_{23}VV$ and KVV lineshapes reveal large differences. These difference are discussed in the context of surface effects, intrinsic and extrinsic plasmon losses, and final state shakeoff. The $L_{23}VV$ and KVV lineshapes also suggest some distortion effects due to final state hole correlation. The $KL_{23}L_{23}$ lineshape is interpreted in the context of similar lineshapes for Na, Mg, Al and P; all show plasmon losses, and except for P, initial state shakeoff contributions.

Originator Supplied Keywords include:)

*Supported by the Office of Naval Research

-2-

(See DD 1473 (Field 12)

1. INTRODUCTION

The Auger process is a complicated dynamical process exhibiting several interesting phenomena (1). One of these is atomic relaxation and electron screening in response to either the initial or final state core holes. In an effort to develop a semiempirical approach to near quantitative Auger lineshape interpretation, we have previously developed a final state rule (FS rule) which provides a simple prescription for including some of the effects of core hole screening in the Auger lineshape (2). In this work, we utilize the FS rule to consistently interpret the CCV, CVV, and CCC (C = core, V = valence) Auger lineshapes of Si.

The well characterized Auger lineshapes of Si provide an ideal system for testing the FS rule and sorting out screening effects in the Auger process. The KL_1V, $KL_{23}V$, $L_1L_{23}V$, and $L_{23}VV$ lineshapes have been extensively studied and reported in the literature (3-9). The KL_1V, $KL_{23}V$, and $L_1L_{23}V$ lineshapes have been shown to exhibit large core hole screening effects, consistent with a final state core hole in these CCV lineshapes (9), but quantitative interpretations of these lineshapes have not been reported in the context of core hole screening (3-8). Much controversy has existed in the literature concerning the interpretation of the $L_{23}VV$ lineshape and the apparent lack of ss and sp contributions (s and p refer to the local angular momentum of the final state valence holes created by the Auger process) to the lineshape (4-8). This lack of ss and sp intensity has been attributed to atomic Auger matrix element effects (4,5,7,8) or to

the nature (local vs. bonding) of the electronic charge sampled by the Auger process (6). In this work we shall attempt to show that the apparent lack of ss and sp contributions in the CVV lineshapes ($L_{23}VV$ and KVV) arises either from the core hole screening response in the initial state or from surface effects. The KVV lineshape to our knowledge has not been previously reported; we present qualitative results for the KVV lineshape in this work (Sec. 2). The $KL_{23}L_{23}$ (CCC) lineshape is obtained also in this work and discussed in the context of core hole screening effects.

The response of the valence electrons to the creation of a core hole can take several forms. In simple atoms, the orbitals usually contract around a core hole, this is normally referred to as atomic relaxation. In molecules and solids, the bonds also polarize, i.e. electron density in a bonding orbital flows toward the core hole, in an antibonding orbital it flows away from the hole. In the event the bonding and antibonding orbitals (bands in the case of a solid) are not completely filled, a net charge transfer to the atom with the core hole results. In some systems the screening charge may be sufficiently polarized as to produce a localized or excitonic state below the valence or conduction band (10-12). The screening may also involve a more non-local accumulation of charge around the core hole (plasmon) or create electron-hole pairs giving rise to an edge singularity (13).

In this work, all of these screening effects are either exhibited in the Si Auger lineshapes and/or included in our theoretical interpretation. The Si Auger lineshapes will be interpreted utilizing the Si theoretical density of states,DOS,

as reported by Papaconstantopoulos and Economou using a Slater-Koster Hamiltonian (Sec. 3) (14). A Green's function approach derived for the tight-binding Hamiltonian is used to distort the ground state DOS giving the proper polarization and charge transfer of the valence electrons in response to the core hole (15). Introducing the OPS rule (the 'orthogonalized' FS rule will be discussed in Sec. 3 but not utilized in this work) accounts for electron hole pair excitations and the edge singularity (2). Plasmon effects are not explicitly accounted for in the theory but are clearly evident in the $KL_{23}L_{23}$ lineshape and perhaps the KVV lineshape. Atomic relaxation introduces initial and final state shake-off. These shakeoff effects must be interpreted as a breakdown in the validity of the FS rule as we applied it in this work, however, they may be included in the OPS rule (2). It is believed final state shakeoff may be exhibited in the CVV lineshapes.

2. EXPERIMENT

The KVV Auger spectrum is normally of extremely low intensity. This arises because a Si K core hole may decay via any of the following Auger processes: $KL_{23}L_{23}$, $KL_{23}V$, KL_1V, and KVV, as well as via X-ray emission. Calculations of Chen et al. indicate the following relative decay rates respectively: 1., 0.02, 0.07, 0.002, and 0.165 (16, 17). Thus roughly only one KVV electron can be expected per 630 K core hole excitations. This small intensity for the KVV lineshape probably accounts for its absence in the literature.

In this work, the KVV lineshape was obtained utilizing the

Physical Electronics model 545 spectrometer. Si samples were cut from a wafer of microelectronics grade. During the data collection, the surface was continuously Ar sputtered at a pressure of 5×10^{-7} torr to prevent a buildup of SiO_x. The Auger process was initiated via electron excitation at 5 KeV and at a current of ~ 10 μA in the normal derivative mode with a modulation potential of 4 Volts. The data was collected from 1765 to 1900 eV over a period of ~ 50 hrs. Despite the high noise level, the peak at ~1846 eV was reproduced in several experiments. A linear background was substracted from the measured $d(EN(E))/dE$ lineshape. This is shown along with a point by point integrated results in Fig. 1; integration smooths the data dramatically. A loss spectrum was taken at Ep ~ 1860 eV and deconvoluted from this integrated spectrum (3, 5-7, 18). The large width of the elastic peak reflects the poor resolution of the single pass CMA ($\Delta E/E$ ~ .005) at these high energies, and makes the normal deconvolution procedure much more difficult. We found that separating the loss spectrum into two parts, the elastic peak and the loss spectrum, and then deconvoluting the loss part first made it possible to remove the loss contributions from the Auger spectrum easily. Deconvolution of the elastic peak was more difficult; and the iterative van Cittert scheme ultimately introduced extraneous peaks (19). This was avoided by terminating the iterative scheme earlier, but we believe most of the resolution broadening was removed.

The Si KLL lineshape was x-ray excited utilizing continuous Bremsstrahlung radiation coming from an Al anode under 5 KeV electron bombardment. The use of continuous Bremsstrahlung

radiation (2#) for Auger excitation has been previously termed continous x-ray excited AES (CXAES) (21, 22), but in reality the Auger process is such that no difference should exist between the CXAES and a normal AES lineshape using a high energy x-ray line source. In Sec. 4, Fig. 11, we compare the Si KLL lineshape obtained in this work with that of Cazaux and Minh Duc (22), who used Bremsstrahlung radiation from a W anode. We have smoothed the published data once and both lineshapes were deconvoluted with a hypothetical flat and constant "loss" function and zero width elastic peak to remove the background due to the non-characteristic extrinsic losses (19). The width of the main line reflects the lifetime of the Si K level, experimental resolution (approximately ~ 1 eV for the McPherson hemispherical analyzer used to take the KLL spectrum in this work), and broadening due to the smoothing procedure.

3. THEORY

3.1 The Final State Rule

The final state (FS) rule for Auger lineshapes (2) is an extension of the FS rule in existence for x-ray emission and absorption (23-25). The FS rule has been previously applied to the CVV Auger lineshapes of Na metal (23c). The FS rule for the Auger process can be stated as follows: in the absence of significant configuration mixing (localization) and shake processes, the initial state determines separately the relative λ or $\lambda\lambda'$ (λ = s or p) Auger intensities; the shape of each contribution is determined by the final density of states (DOS) (2). An 'orthogonalized' FS (OFS) rule also has been derived.

It has been shown to improve on the FS rule primarily near the threshold where it accounts for some of the edge singularity effects (2, 26). The Auger intensity $W(\varepsilon)$ within the FS and OFS rules can be written in terms of the normal Auger matrix elements (2),

$$W_{FS}(\varepsilon) \propto |\langle \Phi_c \bar{\varepsilon}_q | r_{12}^{-1} | \Phi_i \bar{\Phi}_j \rangle|^2 \qquad 1)$$

$$W_{OFS}(\varepsilon) \propto |\langle \Phi_c \bar{\varepsilon}_q | r_{12}^{-1} | \tilde{\Phi}_i \bar{\Phi}_j \rangle|^2 . \qquad 2)$$

The final state holes Φ_i and $\bar{\Phi}_j$ arise as a result of the Auger process; the Auger electron escapes with energy ε_q in the continuum orbital $\bar{\varepsilon}_q$, the other electron drops into the core orbital Φ_c. $\bar{\Phi}$ indicates orbitals with spin down, Φ those with spin up.

In eqs. (1) and (2), Φ_i and $\tilde{\Phi}_i$ are related by the expression,

$$\tilde{\Phi}_i = \Phi_i - \sum_{n(UO)} S_{in} \Phi_n' - \sum_m S_{im} f_{im}' = \sum_{n(O)} S_{in} \Phi_n' , \qquad 3)$$

where Φ_n' are the unoccupied (UO) band orbitals (from the same band as Φ_i) in the presence of the initial state core hole, and the f_{im}' are all the other unoccupied orbitals (Rydberg, continuum etc.) in the potential of the initial core hole (2). In eq. (3), the $\tilde{\Phi}_i$ orbitals are othogonalized to all the unoccupied initial state orbitals, hence the name orthogonalized FS rule. Projecting out the Φ_n' contributions accounts for the particle-hole pair excitations reflected in the edge singularity effects, and the f_{im}' essentially account for atomic relaxation that introduces final state shakeoff. In practice it is easier to

project the ϕ_i onto the occupied (O) initial state orbitals as indicated in eq. (3), but even this procedure requires a reduction of the infinite band orbital problem to a finite number of cluster orbitals (26). In this work, we utilize only the FS rule which does not require the projection procedure, and hence ignore these two screening effects. No edge singularity effects are evident in the Auger lineshapes of Si. We will discuss only qualitatively the final state shakeoff effects evident in the Si CVV lineshapes.

The experimental lineshapes, A(E), are quantitatively examined using the equations,

$$A_{CCV}(E) = C_S N'_S(E) + C_P N'_P \quad (E) \qquad 4)$$

$$A_{CVV}(E) = C_{SS} R_S^2 N_S(E) * N_S(E) + C_{SP} R_S R_P N_S(E) * N_P(E) \qquad 5)$$

$$+ C_{PP} R_P^2 N_P(E) * N_P(E),$$

where $N_\ell(E) * N_{\ell'}(E)$ indicates the fold of the DOS,

$$N_\ell(E) * N_{\ell'}(E) = \int N_\ell(E - \epsilon) N_{\ell'}(\epsilon) \, d\epsilon, \qquad 6)$$

consistent with the FS rule, $N_\ell(E)$ is the DOS of the final state without a core hole, $N'_\ell(E)$ is the screened DOS local to a core hole. The R_ℓ factors in eq. (5) can be defined,

$$R_\ell = \int_{occ} N'_\ell(\epsilon) \, d\epsilon / \int_{occ} N_\ell(\epsilon) \, d\epsilon \quad . \qquad 7)$$

They are the ratio of local charge in the screened initial state to that in the unscreened final state of the CVV Auger process. They appear in eq. (5) because the FS rule states that the relative intensities of the $\ell\ell'$ contributions are determined by the initial state. They do not appear in eq. (4) because both the initial and final states contain a core hole (i.e. the R

factors are assumed to be one). An expression similar to eq. (4) has been used previously to interpret the CCV Auger lineshapes in Na (23d).

Eq. (5) assumes that final state hole-hole correlation effects are negligible in the CVV lineshapes. In the event that correlation effects are not negligible, the $N_\ell(E) * N_{\ell'}(E)$ lineshape becomes distorted, this can be included by using the Cini-Sawatsky expression (see ref. 1 and other references cited there),

$$N''_\ell(E) * N''_{\ell'}(E) = \frac{N_\ell(E) * N_{\ell'}(E)}{(1 - U\, I(E))^2 + U^2 \pi^2 [N_\ell(E) * N_{\ell'}(E)]^2} \qquad 8)$$

where I(E) is the Hilbert transform,

$$I(E) = \int N_\ell(E) * N_{\ell'}(E) / (E - \epsilon) \, d\epsilon \quad . \qquad 9)$$

Above, U is the fully screened hole-hole Coulomb repulsion and $N''_\ell * N''_{\ell'}$ and $N_\ell * N_{\ell'}$ are the correlated and uncorrelated folds of the DOS respectively. We shall see in Sec. 4.2 that small distortion effects are indeed evident in the Si L_{23} VV lineshape.

3.2 Atomic Auger Matrix Elements.

The coefficients C_ℓ and $C_{\ell\ell'}$ are obtained from an optimal fit of the right hand side of eqs. (4) and (5) to the experimental lineshape. The ratio of the coefficients reflects the ratio of the atomic Auger matrix elements,

$$1/3 \; C_S / C_P = A_{CCS} / A_{CCP} \qquad 10)$$

$$1/9 \; C_{SS} / C_{PP} = A_{CSS} / A_{CPP} \qquad 11)$$

$$1/3 \; C_{SP} / C_{PP} = A_{CSP} / A_{CPP}$$

where the numerical factors arise to account for the presence of

3p orbitals (p_x , p_y , p_z) versus just a single s orbital. The atomic Auger matrix elements, $A_{c\gamma\gamma}$ and $A_{cc\beta}$, normalized per filled shell, can be obtained empirically and compared with what the lineshape fit indicates. Such a comparison provides a measure of the overall consistency of our lineshape interpretation technique and, hence, also on the validity of the FS rule used in the interpretation.

Fig. 2 contains plots of the matrix element ratios, $A_{\alpha s}/ A_{\alpha p}$ for the KL_1V, $KL_{23}V$, and $L_1L_{23}V$ lineshapes. We consider just the KL_1V and $KL_{23}V$ plots first. Both theoretical and experimental results are shown. The experimental intensities (except for Ar) have been tabulated by Bakenkov et al. (27) from the literature. The experimental Argon results are from Asplund et al. (28) and Mackey et al; (29), the latter data arising from proton impact rather than electron impact as in all of the other data. Several theoretical calculations of varying degrees of sophistication have also been reported; only the two most recent are shown in Fig. 2. Those of Chen et al. (16) have been calculated ab initio relativistically from perturbation theory, for frozen orbitals, in the Dirac-Hartree Slater approach. Walters and Bhalla (30) utilized a numerical Hartree Fock Slater approach with the Kohn-Sham and Gaspar exchange approximation.

The $L_1L_{23}V$ Koster Kronig (CK) case presents a special problem, both theoretically and experimentally, because of the low CK electron kinetic energy. The low kinetic energy causes the theoretical calculations to show a strong dependence on the estimate of this energy. This has been illustrated for Ar by McGuire (31) using his approximate Herman-Skillman calculations,

where both theoretical model energies and experimental XPS bindings energies were used in the expression,

$$E_{L_1 L_{23} M} = E_{L_1} - E_{L_{23}} - E_M \quad , \quad 12)$$

to estimate $E_{L_1 L_{23} M}$. Large differences were seen in the absolute magnitudes of the CK matrix elements for these two estimates of $E_{L_1 L_{23} M}$. Fig. 2 shows that this causes large differences also in the s/p ratio. More recent theoretical results of Chen et al. (16) are based on relativistic relaxed orbital calculations of $E_{L_1 L_{23} M}$ (32). These calculations are expected to give more realistic CK continuum energies and hence also more realistic s/p ratios. In any event, results for only four different values of Z have been reported for each calculation, and the s/p ratio varies widely over this range. Analysis of the results of Chen et al. (16) reveals this large variation arises for two reasons. The $L_1 L_2 M_1$ process terminates beyond Z = 24, because $E_{L_1 L_2 M_1}$ is negative beyond this point. The $L_1 L_3 M_1$ process terminates beyond Z = 30 for the same reason. Since the $L_1 L_2 M_1$ rate is essentially 1/2 the $L_1 L_3 M_1$ rate in this region, a sharp break in the s/p ratio occurs at Z = 24. We have scaled this out in Fig. 2 by multiplying the s/p ratio by 1.5 above Z = 24. The second reason for the strong s/p variation arises from the total $L_1 L_{23} M_{23}$ rate which seems to increase linearly with Z (16). Thus we plot the Chen et al. (16) results in Fig. 2, using the quantity (s/p)·Z·(1.5 for Z > 24). McGuire's (31) results do not show the drop off of the $L_1 L_2 M_1$ process in this region (different $E_{L_1 L_{23} M}$ were used as discussed above);

therefore McGuire's results are plotted simply as $Z \cdot (s/p)$. Both plots still have an appreciable variation over this narrow range of Z.

The experimental s/p results are equally uncertain because the $L_1L_{23}V$ lineshape at these low kinetic energies lies on top of a large secondary electron contribution. Experimental results exist only for Ar. The results of Mehlhorn (33) obtained from the s/p area ratios in the $L_1L_{23}V$ lineshape are indicated with a large uncertainty to emphasize the background problem. McGuire analyzed the Ar $L_{23}M$-M^3 satellite structure at higher kinetic energies (34). The initial state of these satellites arises from both the $L_1L_{23}M$ Auger process as well as from initial state shakeoff. Based on this analysis McGuire concluded the s/p ratio for Ar is ~0.5, a factor of 2 less than his theoretical estimate and a factor of 2 greater than Mehlhorn's experimental estimate (34). Our best estimate for Si is then obtained using an extrapolation ($Z \cdot (s/p) \approx 30$) of the theoretical results of Chen et al. (16), but scaled by 9/23 to match the experimental result for Ar, i.e. $(s/p)_{Si} \approx (30/14) \times (9/23) \approx 0.8$. This result is indicated in Table 1 along with an estimated large uncertainity.

Similar experimental and theoretical ss/pp and sp/pp plots for the $L_{23}MM$ and KMM processes have been reported elsewhere (1, 17). Whereas the theoretical and experimental results are in excellent agreement for the KL_1M and $KL_{23}M$ lineshapes, large discrepancies are found between the one electron theoretical results and the experimental results for the $L_{23}MM$ and KMM processes (1, 17). This has been attributed to the larger final state electron correlation effects that exist when two holes are

in the same shell. Indeed theoretical results which included electron correlation effects (such as from configuration interaction (CI) calculations) were found to agree nicely with experiment (35-38). Furthermore the one-electron theoretical results for different Z (16, 39, 40) could be scaled (requiring factors of from .6 up to 2.) by a constant factor to give excellent agreement with experiment; this indicates a constant correlation effect (1). The optimal matrix element ratios obtained from extrapolation of these plots are given in Table 1.

3.3 The Screened and Unscreened Valence DOS.

The CVV lineshapes should reflect the final DOS in the absence of a core hole consistent with the FS rule and eq. (5). If the final state holes completely delocalize (1, 4-9), the final state is accurately represented by the ground DOS. We shall use the DOS calculated by Papaconstantopoulos and Economou (14) utilizing the Slater-Koster parameterized tight-binding Hamiltonian constructed using four orthogonal orbitals per site. These can be compared to the KV and $L_{23}V$ x-ray emission spectra (XES) (41), which reflect the ground state p and s DOS respectively, consistent with the FS rule (23-26). This comparison is shown in Figs. 3a and 4a where the occupied theoretical DOS have been broadened with a gaussian of FWHM equal 1.5 eV to account for the experimental resolution and core hole lifetime broadening.

The CCV lineshapes on the other hand reflect a screened DOS, local to the core hole. The Hamiltonian which describes the screened core hole can be approximated within the tight binding

approximation (15),

$$H = \sum_{m \neq \ell} |m\rangle \varepsilon_0 \langle m| + V \sum_{n,m} |n\rangle\langle m| + |\ell\rangle \varepsilon \langle \ell| \,, \qquad 13)$$

where each state $|m\rangle$ is an atomic like orbital centered at site m which form a regular lattice and ε_0 is the energy of an electron at site ℓ in the absence of V. V is the hopping amplitude for transfer of an electron from one site to another. The core hole is located at site ℓ and introduces the pertubation $|\ell\rangle \varepsilon \langle \ell|$ such that the diagonal matrix element $|\ell\rangle H \langle \ell|$ equals $\varepsilon_0 + \varepsilon$. The DOS at the core hole site, $N_\ell(E)$, can be obtained from the DOS at the remaining sites, $N_m(E)$, utilizing Green's function techniques (15), which give

$$N_\ell(E) \qquad \frac{N_m(E)}{(1 - \varepsilon I(E))^2 + \varepsilon^2 \pi^2 N_m^2(E)} \qquad 14)$$

Here I(E) is the Hilbert transform of the DOS,

$$I(E) = \int N_m(\varepsilon)/(E - \varepsilon)\, d\varepsilon \,. \qquad 15)$$

Eqs (14) and (15) are remarkably similar to eqs. (8) and (9) showing that the polarization parameter ε plays the same role in the distortion of N_m as the Coulomb repulsion U plays in the distortion of $N_\ell(E) \neq N_\ell(E)$.

The distortion to $N_\ell(E)$ from $N_m(E)$ can be seen in Fig. 5 for ε equal to 0, 2, 4 and 6 eV utilizing both the s and p DOS as determined by Papaconstantopoulos and Economou (14). The sum of $N_\ell(E)$ up to the Fermi level, ϵ_F, is indicated also; the integral of $N_\ell(E)$ over the occupied and unoccupied DOS of course remains constant. The distortion reflects the polarization of charge (i.e. to the core hole site in the bonding band orbitals and away

in the antibonding band orbitals). The increase in the occupied DOS as ε increases reflects the net charge transfer to the core hole site. Note also the appearance of an increasingly localized state below the valence band and an excitonic-like state beginning to appear at the bottom of the conduction band for the larger ε values in the s DOS.

The polarization parameter ε can be related to the fully screened and relaxed electron core hole attraction. Its value for Si is not known accurately. We can estimate this value for a 2p core hole in the free atom from the $L_1L_{23}M$ electron energies calculated by Chen et al. (32) and the expression

$$E_{L_1L_{23}M} = E_{L_1} - E_{L_{23}} - E_M - \varepsilon. \qquad 16)$$

The XPS atomic binding energies E_{L_1}, $E_{L_{23}}$, and E_M are well known experimentally giving ε_s = 10 eV and ε_p = 6.5 eV. The larger ε_s value compared with ε_p reflects the deeper penetration of the 3s electrons into the core region where they experience less screening of the core hole from the other valence electrons. The polarization energies in the solid should of course be smaller, due to extra-atomic relaxation and screening (42).

The value of ε_s for a 2p core hole in the solid can be obtained by comparison of Fig. 5 with the Si $L_{23}L_{23} - L_{23}V$ XES data (43). The $L_{23}^2 - L_{23}V$ lineshape reflects the screened s DOS, consistent with the FS rule, and selection rules for the x-ray emission process. The best fit to the XES lineshape is obtained with an ε_s value of 4. eV. This comparison is given in Fig. 3b where the occupied theoretical DOS has been folded with a Gaussian of 5.5 eV. This width reflects a component of 1-2 eV

for experimental resolution and lifetime broadening, and a component of 3-4 eV to account for the exchange correlation effects between the core and localized valence holes (9) and other resonant broadening mechanisms (44). It is expected that such exchange correlation effects could broaden the DOS by some fraction of the central cell potential ϵ_s, and hence be of the order of 3-4 EV.

A similar determination of ϵ_p for a 2p core hole in the solid is not possible, since we are not aware of any $KL_{23} - L_{23}V$ XES data, although we know of no reason why it would not be measurable. A reasonable value of ϵ_p can be obtained however by comparison of Fig. 5b with the KL_1V and $KL_{23}V$ Auger data. This comparison suggests that the principal peak in the 2p DOS shifts to 2 eV higher BE in the presence of a core hole. Thus a value of $\epsilon_p \approx 2$ eV is indicated. The DOS obtained from eq. (14) is shown in Fig. 4b after Gaussian broadening by 3 eV. The 3 eV may again be divided into a component of 1-2 eV from experimental resolution and lifetime broadening and a component of 1-2 eV from core-valence exchange correlation etc; the latter component is smaller than in the s DOS because ϵ_p is less than ϵ_s.

The values of ϵ_s and ϵ_p for 1s and 2s core holes cannot be obtained independently, since obviously no XES or AES data exist with a 1s or 2s final state. It can be assumed however that the central cell polarization potential ϵ is the same for all of the core holes within the equivalent cores (EC) (45) or the optical alchemy approximation (46). These approximations

indicate that an atom with a core hole is equivalent to the transmutation of the excited atom into an atom with a nuclear charge Z+1, provided the hole occupies a smaller radius than the electrons in the valence and conduction bands.

Comparison of the binding energy of the Si 2p core exciton with that of the P (Si's Z+1 transmutant) substitutional donor level, however, suggests that there may in fact be a difference between the 1s and 2p core holes. The P- Si donor level is of the Wannier type having a 45 meV binding energy (47) and according to the EC approximation should closely approximate the 1s core exciton in Si. The Si 2p core exciton appears to be of the deeper Frenkel type with an experimental binding energy of 0.15 to 0.8 eV (48-51). Although still under discussion (50), recent resonant photoemission data on Si(111) near the 2p core excitation threshold strongly suggest that the excitonic -like state is sufficiently long lived for the excited electron to participate in the Auger decay or be a spectator to it (i.e. produce resonant photoemission or satellite emission).

Recent calculations by Hjalmarson et al. (51), utilizing the central cell TBA model such as that utilized here, predicts a Γ_{15} type Si 2p core exciton level which lies 0.02 above the band gap. This is in reasonable agreement with our results in Fig. 5 showing an excitonic like state appearing at the bottom of the conduction band in the s DOS. Increasing the central cell potential will eventually cause a deep level below the conduction band edge, but larger values of ϵ_s and ϵ_p are not indicated from a comparison of theory and experiment in the occupied DOS. Many possibilities have been discussed recently to explain the

deep Si 2p excitonic level including intervalley scattering (52), screening of the core-hole self-energy by the electron orbit (53), incomplete electron relaxation (54), and surface effects (49). It is clear that the central cell TBA models, such as that used here which ignore these effects, as well as the long range Coulomb interaction, cannot adequately predict the core exciton binding energy.

The Auger process samples only the occupied DOS, so that the nature of the core exciton and the unoccupied DOS is not reflected in the Auger lineshape. Nevertheless we can check the quality of our unoccupied s and p DOS in the presence of a core hole by comparison with the experimental Si 2p and 1s absorption spectra which reflect these states (48). These comparisons are given in Figs. 3b and 4b and reveal remarkably good agreement. Note that in this case the unoccupied theoretical DOS does not require large Gaussian broadening (~ 0 eV and 1.7 eV to reflect the photon spectral width) because the resonant broadening mechanism (44) and exchange correlation effects (9) occur only in the presence of two holes (core and valence).

It seems clear that in spite of some problem with the core exciton binding energies, we can safely assume the validity of the EC approximation and the central cell TBA model for the occupied DOS of interest in this work (and for the overall unoccupied DOS). Comparison of the theoretical lineshapes with the experimental lineshapes will provide a check on this assumption.

Another check on the consistency of our screened DOS comes

from the total charge transfer. Figs. 3 and 4 indicate an s charge transfer of 0.27 electrons and a p charge transfer of .73 electrons for a total of 1.0 electron. If this result is correct, it reveals the charge transfer of a whole electron to the core hole even in a semiconductor such as Si, where one might have expected somewhat less. Another point is worth noting, Figs. 3 and 4 suggest that the s DOS suffers a much larger distortion than the p DOS; however, the p DOS brings about the larger charge transfer. The larger distortion of the s DOS was already evident from the qualitative work of Lasser and Fuggle (9); and indeed they suggested that as one progressed from left to right in the series Na, Mg, Al, and Si, the charge transfer shifted from mostly s like to p like because the s DOS are becoming increasely filled. Our screened DOS are consistent with this conclusion.

A final check on the screened DOS can be obtained from the total dynamic relaxation energy of the Si 2p core level, $R_D\ (2p)^{Si}$, which will be dominated by the valence-atomic and extra-atomic relaxation terms, $R_D^{a(val)}(2p)$ and $R_D^{ea}(2p)$, respectively (55). In the central cell approximation utilized in this work, the total valence relaxation energy can be approximated from the expression

$$R_D(2p)^{Si} = 2\int_{occ} \varepsilon \left[N_s'(\varepsilon) - N_s(\varepsilon) + N_p'(\varepsilon) - N_p(\varepsilon) \right] d\varepsilon . \qquad (17)$$

This expression and the DOS in Figs. 3 and 4 gives $R_D\ (2p)^{Si}$ equal to 11.9 eV. Theoretical estimates for $R_D^{ea}\ (2p)^{Si}$ ranging from 4.3 to 6.8 eV have been reported as summarized by Bechstedt et al. (55). $R_D^{a(val)}\ (2p)^{Si}$ can be estimated as one-half the static relaxation energy as given by Shirley (56), i.e. $R_D^{a(val)}\ (2p)^{Si}$ ~ 7 eV. Bechstedt gives a result as low as 2.7 eV. Thus estimates

for R_D $(2p)^{5}$ range from 7.4 to 13.8 eV. Our result is at the upper limit of this range which appears most reasonable.

4. RESULT AND DISCUSSION

4.1 CCV Auger Lineshapes

The CCV lineshapes directly reflect the screened DOS consistent with the FS rule. Figs. 6, 7, 8 compare the experimental KL_1V, $KL_{23}V$, and $L_1L_{23}V$ lineshapes with the optimal fit of eq. (4). Small shifts of the experimental spectra by 2.84, 0.7, and 0.4 eV respectively to lower binding energy were needed to obtain optimum agreement with eq. (4). The shifts of less than 1 eV are of the order of the error in the placement of E_q (9). The reason for the large shift required for the KL_1V spectrum is not known, but we doubt whether it has a fundamental basis. Table 1 compares the approximate coefficient ratios with the empirical matrix elements. These results show excellent agreement within experimental uncertainties and provide quantitative support for the applicability of the FS rule to the CCV lineshapes and the central cell TBA model for the occupied DOS.

4.2 CVV Auger Lineshapes

4.2.1. The LVV Lineshape.

The CVV lineshapes should reflect a fold of the ground state DOS consistent with our discussion in Sec. 3.1. Fig. 9 compares the experimental $L_{23}VV$ lineshapes with the optimal fit of eq. (5). The $2p_{3/2}$ binding energy relative to the bottom of the conduction band is well established at 99.84 ± .06

eV from the L_{23} absorption spectrum (48a). This enables the theoretical $L_{23}VV$ Auger energy scale to be accurately determined. The experimental peak energy in N(E) has been determined by several workers on many different Si crystal faces. Examining these results we place the best estimate at 98 ± 1 eV. (3,5,7). This allows a comparison between the theoretical lineshape obtained using eq. (5), and the experimental lineshape on an absolute energy scale. Fig. 9 shows that with these assumptions, the peaks are not in registry and the slope near the top of the lineshapes are different. Actually the onset of the two lineshapes near the Fermi level are in relatively good agreement. This suggests the presence of some distortion due to final state hole-hole correlation effects. Use of eq. (8) applied separately to both the $N_s * N_p$ and $N_p * N_p$ folds and a U of 1.8 eV provides excellent agreement with experiment. The U of 1.8 eV is reasonable compared with 3.5 - 4 eV in the σ bonds of graphite (a semi-metal) (57) and ~0 eV on the C atom in the pp band of transition metal carbides (conductors) (58).

In Fig. 9, the coefficients C_{ss}, C_{sp}, and C_{pp} of eq. (5) are optimized for the U = 1.8 eV distorted lineshape and forced to be the same for the U = 0 undistorted lineshape. This allows a simple visual determination of the effects of hole-hole correlation. Optimization of the $C_{ll'}$ coefficients for the undistorted (U = 0) folds improved the fit somewhat, but could not give a satisfactory fit to the experimental lineshape.

A similar self-fold of the DOS and comparison with the LVV lineshape for Al shows just the opposite situation from that for

Si, that is the peak in the self-fold appears further down from the Fermi level than in the experimental lineshape (59-62). This clearly indicates that hole-hole correlation effects are much less important in Al than in Si, as one might expect for a metal. In Al, inclusion of surface effects, due to the small sampling depth of the LVV electrons, has been suggested as a mechanism which will shift the theoretical peak back up towards the Fermi level and in registry with experiment (59-62). Near the surface, calculations show that the ss and sp components should be reduced, thus having the effect of increasing the relative importance of the pp component, which has its peak nearer the Fermi level (60, 62).

Including surface effects in the self-fold of the pp DOS for Si also causes the LVV peak to occur closer to the Fermi level (8), suggesting that if these effects were included, an even larger U for Si would be required to lower the peak back to its experimental position. Thus localization effects are indicated in Si; however, uncertainities in the exact placement of the LVV lineshape make it impossible to determine accurately the value of U. Indeed, it should be mentioned that previous comparisons of the empirically (e.g. using the K_β XES spectrum) calculated lineshapes with the experimental LVV lineshape, gave good agreement in the peak positions, as well as in the slopes of N(E) above the main peak (4-8). Evidently, ones conclusions can easily be affected by the placement of the energy scale, and the exact nature of the calculated DOS. Our results for Si are consistent with those recently reported for graphite, Al, and

other conductors and insulators as discussed above, but localizations effects in the Si LVV lineshape cannot be positively identified under these circumstances.

Although excellent agreement between theory and experiment is found in Fig. 9, Table I reveals that the coefficient ratios from the best U = 1.8 eV fit does not at all agree with the empirical matrix element ratios. This arises even though the L_{23} VV matrix element ratios are well established. The apparent near lack of ss and sp contributions in the L_{23} VV lineshape indicated in Table 1 and Fig. 9 is well known, indeed we include previous results of Kunjunny et al. (8) in Table 1 for comparison. The R factors have not been included in the work of Kunjunny et al. (8). The R factors improve the situation, but by less than 10%.

The substantial decrease of the ss and sp contributions suggests that for some reason major parts of the *s* DOS is not sampled by the Auger process. Jennison (6) has shown that because the interatomic s-s overlap is significantly larger than the p-p overlap, the s DOS contributes a significantly greater portion to the bonding charge. He further indicates that the bonding charge is not sampled by the Auger process. The Si 3s orbitals are known to be relaxed and radially extended in the solid relative to that in the free atom (63) and this does increase the interatomic s-s overlap in the ground state. However, in the presence of a core hole, the 3s orbitals are expected to radially contract back to what they were in the free atom, and according to the FS rule the $\ell\ell'$ relative intensities are dictated by the screened core hole initial state. Furthermore, previous

examination of this bonding charge contribution on the Auger lineshapes of equally covalent systems such as NO_3^-, PO_4^{3-}, SO_4^{2-}, (1, 64, 65) and Pd_4Si (66, 67) did not reveal a significant effect. Thus we do not believe that the bonding charge concept is the sole mechanism for the reduced ss and sp components, although it could be partially responsible.

We proposed previously (68) that the lack of the ss and sp contributions in both lineshapes could arise because of the atomic relaxation of the Si 3s orbitals mentioned above, and the final state shakeoff this should introduce. The large difference in the radial extent of the 3s orbital in the screened and unscreened state means a large contribution (i.e. the Si f' contribution in eq. (3)) must be projected or orthogonalized out of the s DOS when utilizing the Orthogonalized FS rule. This 'projected out' portion of the s DOS must also be projected out of the normal Auger lineshape and is redistributed at lower energy, over a wide energy range, as intrinsic loss. This intrinsic loss contribution if present cannot be distinguished from the normal extrinsic loss and so it is taken out as background. A large final state shakeoff or intrinsic loss contribution indicates a breakdown in the FS rule (2), eq. (1), but it arises naturally in the orthogonalized FS rule if the f' terms are included in eq. (3). We have indicated previously (Sec. 3.1) that the orthogonalized FS rule cannot be easily applied quantitatively, and hence it is not attempted here.

4.2.2 The KVV Lineshape

Our primary motivation for measuring the KVV lineshape was

to determine if the ss and sp contributions are extremely small here as well. The extremely weak intensity of the KVV lineshape and the poor energy resolution of the CMA at this high KVV kinetic energy prevented us from accurately determining the lineshape. Nevertheless, it is clear from comparison of Figs. 9, and 10 that the LVV and KVV lineshapes are qualitatively different.

The intensity in the experimental KVV lineshape immediately above the main peak is probably due to an autoionization process $K\bar{E} - V$, where $\bar{E}$ denotes an "excitonic-like" electron in the conduction band as mentioned in Sec. 3.3. This autoionization contribution is larger in the KVV lineshape than in the LVV lineshape probably because of the shorter lifetime of the K core level. Some evidence also exist in the KLV lineshapes (especially in the KL_1V lineshape) for contributions from this process. The small features between 1850-1880 eV are attributed to KL_{23}- $L_{23}VV$ shakeup satellites similar to those recently reported above the Mg $KL_{23}V$ lineshape (69). The structure between 1770 and 1790 eV in Fig. 1 could arise from similar satellites above the Si $KL_{23}V$ lineshape.

The large difference between the KVV and LVV lineshapes below the major peaks has two possible interpretations. First it could mean that the ss and sp contributions indeed are present in the KVV lineshape. To test this, we have applied Eq. (5) to the experimental KVV lineshape assumming $U_{pp} = 2$ as determined for the LVV lineshape. In addition, U_{ss} and U_{sp} were allowed to be free parameters to obtain the best fit of Eq. (5) to the

experimental lineshape. Values of U_{ss} = 6 and U_{sp} = 4 eV were obtained along with the coefficient ratios given in Table 1. The large values of U_{ss} and U_{sp} are not inconsistent with that found in the KVV lineshapes of the transitions metal carbides (58). Furthermore, Table 1 indicates that the ss and sp coefficient ratios are too small, but not all the experimental intensity around 1810 eV is accounted for by the theory as shown in Fig. 10. An improved agreement between the theoretical and experimental lineshapes between 1800 and 1820 eV would then indicate a larger ss and sp coefficient ratio and provide better agreement in Table 1.

A possible expalantion for the poor agreement between theory and experiment near the lower end of the spectrum is that dynamic screening of the valence holes could be important. Recently, Cini has extended his hole correlation theory, as contained in Eq. (8), to include electron screening from the remaining sea of electrons in the valence bands (70). Whereas, Eq. (8) incorporates the "static" screening by utilizing an effective U, the new theory begins with the unscreened U, and includes the dynamic screening directly in the calculations. Unfortunately, this is much more difficult to apply numerically to our DOS, but Cini has shown that for a model DOS, the effect of the dynamic screening is to introduce intrinsic plasmon loss contributions at the bottom of the lineshape. Earlier work has indeed shown that an intrinsic plasmon loss peak is expected below the LVV spectrum in Al (62).

It is important to realize that the losses mentioned above are intrinsic to the Auger lineshape and must be accounted for by

the ss and sp contributions. This is in contrast to the extrinsic losses resulting from inelastic collisions the Auger electrons suffer on their way out of the solid. The extrinsic losses should be removed from the Auger lineshape in the deconvolution procedure, although there is some question as to whether Auger and primary electrons suffer similar loss processes (71). The energy separation in Fig. 10 between the "intrinsic loss contribution" and the main peak, ~ 15 eV, is reasonably consistent with the known bulk plasmon energy of 17 eV (22). This gives the second explanation. All or some of the intensity below 1820 eV could result from unremoved extrinsic plasmon losses, a definite possibility considering the experimental problems with the KVV lineshape.

We believe that at least some of the intensity around 1810 eV arises from intrinsic losses, but it is impossible to determine whether the complete ss and sp contributions are present in the Si KVV lineshape or not. And why are similar intrinsic loss contributions apparently not present in the Si LVV lineshape. The extreme surface sensitivity of the ~ 90 eV LVV electrons could cause a reduction in the intrinsic plasmon component, but this is only speculation.

4.2.3 Comparison With Other Systems

Data for the neighboring elements Mg, Al, and P are equally uncertain. Recently Davies et al. (72) reported the KVV lineshape for Mg and compared it with the previously reported LVV lineshape (71). They concluded that both lineshapes similarly are missing large portions of the ss and sp components, and that

the small differences between the lineshapes could be accounted for by the different matrix element ratios between the LVV and KVV processes as shown in Table 1. However, both the KVV and LVV lineshapes (in this case the LVV does have a plasmon loss but apparently still smaller than the KVV) have plasmon losses just below the main lineshapes, and uncertainties in removing this intensity exist in both cases so that the presence of intrinsic losses have not definitely been established (71, 72). Furthermore, the sp and pp spectral lineshapes in Mg are similar, making it rather difficult to determine their exact relative contributions by the curve fitting procedure of Davies et al., a procedure very similar to that indicated by Eq. (5). Interpretations of the LVV lineshape for Al, and P also indicate sharp reductions in the ss and sp contributions (60-62, 73). The KVV lineshapes for Al and P to our knowledge have not been reported.

If the ss and sp contributions are fully reflected in the KVV lineshape, but not in the LVV lineshapes of these four elemental solids, then final state shakeoff is most likely not the cause of the ss and sp reductions in the LVV lineshapes, since final state shakeoff is expected to be equally active in both the LVV and KVV lineshapes (74). In this case, one could speculate that the differences in mean free paths of the high energy KVV electrons vs. the small energy of the LVV electrons causes the differences. It has been proposed that the dangling bonds at the surface in Si are primarily p-like with the back-bonds of the surface Si atoms primarily sp^2 like (75). An

extremely short sampling depth of the LVV Auger process (i.e. sampling primarily the p-like dangling bonds and only part of the sp^2 backbonds) would then explain the predominance of pp like character in the LVV lineshape. Calculations on Al metal also shows that the surface layers have more p-like character than the bulk, and indeed this has been proposed previously to explain the reduction of the ss and sp components in the Al LVV lineshape (60-62).

If both the KVV and LVV lineshapes have reduced ss and sp components, as indicated by Davies et al for Mg, and perhaps may also be the case for Si, Al, and P, then we propose final state shakeoff as a primary cause as explained above. These elemental solids would then provide the first instance to our knowledge where final state shakeoff causes large changes in the Auger spectral lineshape. The total Auger integrated intensity should also reflect this loss in intensity. However a quantitative determination of the experimental Auger intensity is difficult; a determination of the shakeoff in this manner would require an accurate knowledge of the excitation cross-section, the mean free path, and a host of other parameters (76). A comparison of the relative total S L_{23} VV Auger intensity from Ag_2S and Ag_2SO_4 has been utilized recently to indicate a large final state shakeoff contribution arising from atomic 3d orbital relaxation in Ag_2SO_4 (77). The diffuse S 3d orbitals are not occupied in Ag_2S, so that the intrinsic loss process does not occur in Ag_2S. Final state shakeoff is difficult to observe even in the gas phase because it is so difficult to distinguish the intrinsic and extrinsic loss processes; however, final state shakeup, which can

produce satellite peaks in the gas phase spectrum, has been observed recently in the Auger lineshape of atomic Mg (78).

Initial state shakeoff, arising from ionization of the initial core electron, does not cause loss of intensity but rather shifts intensity throughout the normal Auger lineshape. In the gas phase, this is seen as additional satellite peaks; they are very prevalent (up to 30% or even more of the total intensity) in most atomic Auger spectra (e.g. in Ar (34), Na (79,80), and Mg 81,82). In the solid, this is seen as additional intensity somewhat shifted from the parent lines but rarely individually resolved from the parent intensity (65). In general, one can expect approximately the same amount of final state shake, as initial state shake since in each case the probability for shake, P_s , can be related to the square of the overlap between the core hole screened, ψ' , and unscreened, ψ , many electron wavefunctions, i.e. $P_s = 1 - \langle \psi | \psi' \rangle^2$ (83). In the sudden approximation it makes no difference whether Ψ or Ψ' is the initial state. Recent experimental and theoretical studies (84) of the transition from adiabatic to sudden excitation indicates the sudden approximation is valid at surprisingly low energies, indicating it may be reasonably valid for the CVV Auger processes of Si. The initial state shakeoff process may be aborted in the covalent systems if the valence and core holes do not remain localized. This is expected to occur in Si for valence state shakeoff (1). Thus little initial state shakeoff is seen or expected in the Si CVV lineshapes, only final state shakeoff is possible.

In summary, final state shakeoff and intrinsic plasmon loss are both intrinsic to the Auger process and both result from a screening response by the remaining valence electrons. Final state shakeoff results in a loss of Auger intensity (i.e. it is removed as background), intrinsic plasmon loss shifts Auger intensity down into a plasmon peak which is difficult to distinguish from extrinsic plasmon loss (i.e. the extrinsic and intrinsic contributions may or may not be removed in the deconvolution process). Under these conditions it is impossible to prove the existence of either process.

Furthermore, the existence of surface reconstruction effects is also difficult to prove. Further work is required on these CVV lineshapes to establish the role of these processes. However, based on all of the present KVV and LVV data for Si, Al, Mg, and P, we currently think that intrinsic plasmon loss effects are important in the KVV lineshapes, and surface effects play a large role in the LVV lineshapes. Furthermore, final state hole correlation effects are present in both lineshapes, particularly in the ss and sp components of the KVV lineshape.

4.3 CCC Auger Lineshapes

We examine only the $KL_{23}L_{23}$ Auger lineshape of the various possible CCC lineshapes. It obviously does not reflect the valence DOS, but screening effects are visible. The $KL_{23}\ L_{23}$ lineshape is interpreted in the context of similar interpretations of this lineshape for Na (85), Mg (86-88), and Al (89) metals, and for P (90), an insulator. These flank Si in the periodic table and provide an ideal series for comparison.

However, Si is the only semi-conductor in this series and might have different screening properties that could be reflected in the $KL_{23}\ L_{23}$ lineshape.

Table 2 contains a comparison of the intensity and energy of various features in the lineshape relative to the main ^1D peak. All five lineshapes show a bulk plasmon loss peak with the relative intensity of Si and P about 1/2 those of the three metals, probably reflecting the loss of free-electron character in Si and P. The bulk plasmon loss energy, E_B, increases by almost 5 eV with each increase in Z. On the other hand, the ^1S and shakeoff peak energy shifts are relatively constant. This causes the KLL spectra to significantly change in appearance as the plasmon loss peak sweeps through the ^1S and shakeoff peaks with increasing Z. The shakeoff peak at -7 to - 10 eV is clearly resolved in the Na data and has been interpreted as due to the $KL\text{-}LL^2$ processes (85). These peaks are visible in the published Mg and Al data; however they are not specifically mentioned by van Attenkum and Trooster (86, 89) and their intensity cannot be quantitatively determined because of interference with the plasmon peaks. It is not visible in P (90). In Fig. 11 for Si, a similar shakeoff contribution is visible in the data of Cazaux and Minh Duc (22) (it is also clearly visible in the data of Taylor (91) not shown in Fig. 10). It is not resolved in our data, although it may be present around 1604 eV.

The $KL\text{-}LL^2$ shakeoff contribution arises from initial state shakeoff. The KL holes do not delocalize because in this case both holes are core like (MM holes do delocalize before the Auger

process and hence do not produce satellites in the solid (1)). The probability for $L_1 + L_2 + L_3$ shakeoff as a result of β - decay has been estimated by Carlson et al. (83) utilizing Hartree Fock atomic wavefunctions and the sudden approximation. This theoretical probability varies linearly with Z as indicated in Table 2. An analysis of atomic Auger data for atomic Na (79 - 81) and Mg (82, 83) indicates the shakeoff probability is in remarkably good agreement with these theoretical results. Data from covalent molecular gases indicates the molecular environment does not alter significantly the shakeoff probability (as opposed to the shakeup probability that does vary (92)). Although further work is required before one can draw any firm conclusions about shakeoff probabilities in these covalent solids, the relative shakeoff probabilities are in reasonable agreement with those predicted by the theory.

The energy shift $E_{KL\text{-}L^3} - E_{KLL}$ can be estimated from the expression (93, 64),

$$\Delta E_{KL\text{-}L^3} = E_{KL\text{-}L^3} - E_{KLL} = (E_K + E_L + U_{KL} - 3E_L - 3U_{LL}) - (E_K - 2E_L - U_{LL}) = U_{KL} - 2U_{LL} \qquad (8)$$

where pairwise additivity of the three L final state holes has been assumed. The latter approximation has been shown to be reasonable for valence holes in atoms and even in molecules and molecular oxyanions (1, 64, 65). In the latter systems, U_{XY} was calculated assuming delocalization of the holes about the molecular system. In the Na - P series, the three core holes are definitely localized on the same atom, however large interatomic screening effects will definitely reduce the three hole repulsion

from the estimate ($3U_{LL}$) dictated by pairwise additivity. Thus interatomic screening will decrease ΔE_{KL-L^3} which accounts for the smaller experimental shakeoff shifts in Table 2. U_{LL} and U_{KL} in eq. (15) can be estimated from the expressions,

$$U_{LL} = E_K - 2E_L - E_{KLL} \qquad 19)$$

$$U_{KL} = E_L^{Z+1} - E_L^{Z} \quad , \qquad 20)$$

utilizing XPS binding energies (83) and the KLL (^1D) Auger kinetic energies in Table 2. Eq. (20) arises in the equivalent cores approximation (45).

5. SUMMARY AND CONCLUSIONS

We have used a previously published theoretical DOS for Si and a Green's function approach to distort these DOS appropriate for a screened core hole. We have compared these distorted DOS with XES and AES data to determine the central cell potentials ϵ_s and ϵ_p, and found that although the s DOS more significantly changes its appearance, more of the charge transfer occurs through the p orbitals. We have used this screened and unscreened DOS and the final state rule to quantitatively interpret the CCC, CCV, and CVV Auger lineshapes of Si. The results of this work lead to the following conclusions:

1) The KL_1V, $KL_{23}V$, and $L_1L_{23}V$ lineshapes reflect the final state core-hole screened DOS consistent with the final state rule.

2) The $L_{23}VV$ and KVV lineshapes are qualitatively different. This difference is discussed in the context of surface effects, intrinsic and extrinsic plasmon losses, and final state shakeoff.

3) All features in the $KL_{23}L_{23}$ lineshape of Si are consistent with the same features in the lineshapes for Na, Mg, Al, and P.

4) Core hole screening (i.e. charge transfer and polarization, initial and final state shakeoff from atomic relaxation, and plasmon loss) inherently affects the Auger lineshapes of Si, and must be included in a quantitative interpretation of the lineshapes.

ACKNOWLEDGEMENTS

We acknowledge receiving helpful suggestions from Carter White concerning the theoretical DOS, and from Jim Murday concerning the experimental data in this work.

TABLE I Comparison of the Atomic Auger Matrix element Ratios

Lineshape		Coefficient Ratio[a]	Theory & Exp. Data[b]	
KL V	s/p	.79	.75	.1
KL V	s/p	.23	.3	.1
L L V	s/p	.64	.8	.4
L VV	ss/pp	.0086	.025	.001
		(.0007)[c]		
	sp/pp	.052	.38	.02
		(0.073)[c]		
KVV	ss/pp	.090	.15	.02
	sp/pp	.294	.46	.02

[a] Matrix element ratios (e.g A_{ccs} / A_{ccp}) obtained from the fit of eqs. (4) and (5) to the experimental lineshapes.

[b] Estimated results and uncertainities from Fig. 2 and refs. 1 and 17 as discussed in the text.

[c] Results of Sunjunny et al (8) obtained without the inclusion of the R factors in Eq. (5).

Table 2 Comparison of KL_{23} L_{23} Spectral Features in Na, Mg, Al, P, and Si[a]

PARAMETER	Na[b]	Mg[c]	Al[d]	Si[e]	P[f]
E_B (eV)	5.8 ± .05	10.6 ± .2	15.5 ± .2	17.2 ± 1.	19.4 ± .5
$I_B/I(^1D)$	.65 ± .05	.84 ± .03	.82 ± .02	.33 ± .07	.48 ± .05
$\Delta E(^1D-^1S)$, eV	4.5 ± .1	5.4 ± .4	6.1 ± .4	6.9 ± .1	5.7 ± .6
		(6.0)[g]	(6.9)[h]		(6.9)[i]
$I(^1S)/I(^1D)$	ND	.2 ± .1	.2 ± .1	.16 ± .01	.11 ± .02
	(.124)[j]	.153 ± .03[k]			(.12)[ℓ]
ΔE_{KL-L^3}, eV	-7.5 ± .1	-9 ± 1	-9 ± 1	-10.5 ± .1	not obs.
	(-13.2)[m]	(-12.6)[m]	(-14.1)[m]	(-17.5)[m]	
I(SO)/ $I(^1D)$	.09 ± .01	ND	ND	.05 ± .01	not obs.
	(.152)[n]	(.108)[n]	(.083)[n]	(.065)[n]	(.049)[n]
KLL (^1D), eV	994.3 ± .3	1185.9 ± .2	1393.2 ± .2	1616.5 ± .2[o]	1857.3 ± .2

[a] Results in parentheses correspond to theoretical results

[b] Ref 85 [c] Ref 86 [d] Ref 89 [e] Ref 22 & this work [f] Ref 90

[g] Ref 95 [h] Ref 96 [i] Ref 90 [j] Ref 85 [k] Ref 82 [ℓ] Ref 97

[m] Determined from eq. (18 - 20) as discussed in text.

[n] Ref 83 [o] Ref 98

ND = not determinable because of interference by other peaks.

REFERENCES

1. D. E. Ramaker, "Chemistry and Physics of Solid Surface IV", Springer Series Chem. Phys. 20, ed. by R. Vanselow and R. Howe (Springer, Berlin, 1982), p. 19.

2. D. E. Ramaker, Phys. Rev. 25, 7341 (1982).

3. J. E. Houston, G. Moore and M. G. Lagally, Solid State Commun. 21, 879 (1977).

4. P. J. Feibelman, E. J. McGuire, and K. C. Pandey, Phys. Rev. B15, 2202 (1977); Phys. Rev. Lett. 36, 1154 (1976); P. J. Feibelman and E. J. McGuire, Phys. Rev. B17, 690 (1978).

5. R. Weissmann, W. Schnellhammer, R. Koschatzky, and K. Muller, Appl. Phys. 14, 283 (1977).

6. D. R. Jennison, Phys. Rev. Lett. 40, 807 (1978); Phys. Rev. 18, 6865 (1978).

7. R. H. Brockman and G. J. Russell, Phys. Rev. B22, 6302 (1980).

8. T. Kunjunny and D. K Ferry, Phys. Rev. 24, 4593 (1981); 24, 4604 (1981).

9. R. Lasser and J. C. Fuggle, Phys. Rev. 22, 2637 (1980).

10. N. D. Lang and A. R. Williams, Phys. Rev. B20, 1369 (1979); 16, 2408 (1977); A. R. Williams and N. D. Lang, Phys. Rev. Lett. 40, 954 (1978).

11. K. Schonhammer and O. Gunnarson, Solid State Commun. 23, 691 (1977).

12. G. D. Mahan, Phys. Rev. 163, 612 (1967).

13. J. W. Gadzuk, J. Electron Spectros. Relat. Phenon. 11, 355 (1977).

14. D. A. Papaconstantopoulos and E. N. Economou, Phys. Rev. B22, 2903 (1980).

15. E. N. Economou, "Green's Functions in Quantum Physics", Solid-State Sciences, Vol. 7 (Springer, Berlin, 1979).

16. M. H. Chen, B. Crasemann, and H. Mark, Atomic Data Nuclear Data Tables, 24, 13 (1979); Phys. Rev. 21, 436 (1980).

17. M. I. Babenkov, B. V. Bobykin, and V. S. Zhdanov, J. Electron. Spectrosc. Related Phenom. 31, 307 (1983).

18. D. E. Ramaker, J. S. Murday, and N. H. Turner, J. Electron Spectrosc. Related Phenom. 17, 45 (1979).

19. H. H. Madden and J. E. Houston, J. Appl. Phys. 47, 3071 (1976).

20. R. H. Pratt, Comments Atom Mol. Physics 10, 121 (1981).

21. V. S. Sandararn, J. D. Rogers, and R. Landers. J. Vac. Sci., Technol. 19, 117 (1981).

22. J. Cazaux and T. Minh Duc, J. Electron Spectrosc. Related Phenom. 31, 13 (1983).

23. U. Von Barth and G. Grossman, Solid State Commun. 32, 645 (1979); Phys. Scr. 21, 580 (1980); Phys. Rev. B25, 5150 (1982), Phys. Scr. 28, 107 (1983).

24. G. D. Mahan, Phys. Rev. B21, 1421 (1980).

25. V. I. Grebennikov, Y. A. Babanov, and O. B. Sokolov, Phys. Status Solid 88, 73 (1977).

26. L. C. Davis and L. A. Feldkamp, Phys. Rev. B23, 4269 (1981).

27. M. I. Babenkov, B. V. Bobykin, V. S. Zhdanov, and V. K. Petukhov, Izv. Akad. Nauk 40, 2065 (1976).

28. L. Asplund, P. Kelfve, B. Blomster, H. Siegbahn, and K. Siegbahn, Physica Scripta 16 268 (1977).

29. J. J. Mackey, L. E. Smith, B. M. Johnson, C. P. Moore, and D. L. Matthews, J. Phys. B7, L447 (1974).

30. D. L. Walters and C. P. Bhalla, Atomic Data 3, 301 (1971).

31. E. J. McGuire, Phys. Rev. 3, 1801 (1971).

32. M. H. Chen, B. Crasemann, K. N. Huang, M. Aoyagi, and H. Mark, Atomic Data Nuclear Data Tables 19, 99 (1977).

33. W. Mehlhorn, Zeits. Phys. 208, 1 (1968).

34. E. J. McGuire, Phys. Rev. A11, 1880 (1975).

35. C. P. Bhalla, Phys. Letters 44A, 103 (1973).

36. D. Chattarji and B. Talukdar, Phys. Rev. A7, 42 (1973).

37. M. H. Chen, B. Crasemann, and H. Mark, Phys. Rev. A8, 7, (1973).

38. M. H. Chen, B. Crasemann, and H. Mark, Phys. Rev. A21, 442 (1980).

39. E. J. McGuire, Phys. Rev. 185, 1 (1969); Sandia Laboratory Research Report SC-RR-710875, March 1971 (Unpublished), Phys. Rev. A3, 587 (1971).

40. D. L. Walters and C. P. Bhalla 4, 2164 (1971).

41. G. Wiech and E. Zopf in Band-Structure Spectroscopy of Metals and Alloys, ed. by D. J. Fabian and L. M. Watson (Academic, London, 1973), p. 173.

42. L. Ley, F. R. McFeely, S. P. Kowa iczyk, J. G. Jenkin, and D. A. Shirley, Phys. Rev. B11, 600 (1975); R. Fellenberg, P. Streubel, and A. Meisel, Phys. Stat. Sol. 112, 55 (1982).

43. W. F. Hanson and E. T. Arakawa, Z. Phys. 251, 271 (1972).

44. C. Cini and A. D' Andrea, J. Phys. C 41, 4469 (1983).

45. W. L. Jolly and D. N. Hendrickson, J. Amer. Chem. Soc. 92, 1863 (1970).

46. J. D. Dow, D. R. Franceschetti, P. C. Gibbons, and S. E. Schnatterly, J. Phys. P5, L211 (1975).

47. R. L. Aggarwal, P. Fisher, V. Mourzine, and A. K. Ramdas, Phys. Rev. 138A, 882 (1965).

48. F. C. Brown and O. P. Rustgi, Phys. Rev. Lett. 28, 497 (1972) M. L. Knotek, G. M. Loubriel, R. H. Stulen, C. E. Parks, B. E. Koel, and Z. Hussain, Phys. Rev., B26, 2292 (1982).

49. G. Margaritondo and J. E. Rowe, Phys. Lett. 59A, 464 (1977). R. S. Bauer, R. Z. Bachrach, D. E. Aspnes, and J. C. McMenamin, Nuovo Cimento B39, 464 (1977).

50. K. L. Kobayashi, H. Daimon, and Y. Murata, Phys. Rev. Lett. 50, 1781 (1983); 52, 1569 (1984); R. A. Riedel, M. Turowski, G. Margaritondo, and P. Perfetti, Phys. Rev. Lett. 52, 1568 (1984).

51. H. P. Hjalmarson, P. Vogl, D. J. Wolford, and J. D. Dow, Phys. Rev. Lett. 44 810 (1980); H. P. Hjalmarson, H. Buttner, and J. D. Dow, Phys. Rev. B24, 6010 (1981).

52. L. Resca, L. Resta, and B. Shore, Phys. Rev. B25, 4031 (1982); L. Resca and R. Resta, Phys. Rev. B25, 4038 (1982).

53. A. Zunger, Phys. Rev. Lett. 50, 1215 (1983); V. A. Singh, A. Zunger and V. Lindefelt, Phys. Rev. B27, 1428 (1983).

54. G. Strinati, Phys. Rev. Lett. 49, 1519 (1982).

55. F. Bechstedt, R. Enderlein, R. Fellenberg, P. Streubel, and A. Meisel, J. Electron. Spectrosc. Related Phenom. 31, 131 (1983).

56. D. A. Shirley, Phys, Rev. A7, 1520 (1973); Chem. Phys. Lett. 17, 312 (1972).

57. D. E. Ramaker, F. L. Hutson, R. R. Rye, J. E. Houston, and J. W. Rogers, Jr., J. Vac. Sci. Technol, A2, 1146 (1984); also to be published.

58. P. Pehrsson and D. E. Ramaker, to be published.

59. C. J. Powell, Phys. Rev. Lett. 30, 1179 (1973).

60. J. W. Gadzuk, Phys. Rev. B 9, 1978 (1974).

61. J. E. Houston, J. Vac. Sci. Technol. 12, 255 (1973).

62. J. Pitchek and S. M. Bose, Phys. Lett. 54A, 460 (1975).

63. J. R. Chelikowsky and M. L. Cohen, Phys. Rev. B10, 5095 (1974).

64. F. L. Hutson, D. E. Ramaker, B. I. Dunlap, J. D. Ganjei and J. S. Murday, J. Chem. Phys. 76, 2181 (1982).

65. B. I. Dunlap, F. L. Hutson, D. E. Ramaker, J. Vac. Sci. Technol. 18, 556 (1981).

66. S. D. Bader, L. Richter, M. B. Brodsky, Solid State Commun. 37, 729 (1981).

67. G. W. Rubloff, P. S. Ho, J. F. Freeouf, J. E. Lewis, Phys. Rev. B23, 4183 (1981).

68. D. E. Ramaker, W. N. Mei, and N. H. Turner, J. Vac. Sci. Technol. 20, 563 (1982).

69. M. Davies, D. R. Jennison, and P. Weightman, J. Phys. C: Solid State Phys. 17, L187 (1984).

70. M. Cini and A. D'Andrea, Phys. Rev. B29, 6540 (1984); M. Cini Phys. Rev. 17, 2486 (1978).

71. A. M. Baro and J. A. Tagle, J. Phys. F : Metal Phys. 8, 563 (1978).

72. M. Davies, D. R. Jennison, and P. Weightman, Phys. Rev. B29, 5313 (1984).

73. M. Taniguchi, S. Suga, M. Seki, H. Sakamoto, H. Kanzaki, Y. Akahama, S. Endo, S. Terada, and S. Narita, Sol. State Commun. 49, 867 (1984).

74. M. O. Krause, T. A. Carlson, and R. D. Dismukes, Phys. Rev. 178, 37 (1968); T. A. Carlson, Radiation Res. 64, 53 (1975).

75. D. Haneman, Phys. Rev. 121, 1093 (1961); D. J. Miller and D. Haneman, J. Vac. Sci. Technol. 16, 1270 (1979).

76. M. P. Seah, "Auger Electron Spectroscopy", National Physical Laboratory Report, DMA(A) 40, February 1982 (Unpublished).

77. N. H. Turner and D. E. Ramaker, J. Vac. Sci. Technol. 1, 1229 (1983).

78. B. Breuckmann, J. Phys. B12, L689 (1979).

79. E. Breuckmann, B. Breuckmann, W. Mehlhorn, and W. Schmitz, J. Phys. B10, 3135 (1977).

80. D. Petrini, Astron. Astrophys. 111, 279 (1982).

81. B. Breuckmann and V. Schmidt, Z. Physik 268, 235 (1974) B. Breuckmann and V. Schmidt, and W. Schmitz, J. Phys. B9, 3837 (1976).

82. N. Kosugi and H. Kuroda, Chem. Phys. Lett. 87, 365 (1982).

83. T. A. Carlson, C. W. Nestor, Jr., T. C. Tucker, and F. B. Malik, Phys. Rev. 169, 27 (1968).

84. J. Stohr, R. Jaeger, and J. J. Rehr, Phys. Rev. Lett. 51, 821 (1983); T. D. Thomas, Phys. Rev. Lett. 52, 417 (1984).

85. A. Barrie and F. J. Street, J. Elect. Spect. Related Phenom 1, 1, (1975).

86. P. M. Th. M. van Attekum, and J. M. Trooster, Phys. Rev. 20, 2335 (1979).

87. A. Fahlman, R. Nordberg, C. Nordling and K. Siegbahn, Z. Phys. 192, 476 (1966).

88. J. C. Fuggle, L. M. Watson, D. J. Fabian, and S. Affrossman, J. Phys. F5, 375 (1975).

89. P. M. Th. M. van Attekum and J. M. Trooster, Phys. Rev. 18, 3872 (1978).

90. M. Scharli and J. Brunner, Z. Phys. B42, 285 (1981).

91. J. A. Taylor, Appl. Surf. Sci. 7, 168 (1981).

92. H. J. Freund, E. W. Plummer, W. R. Salaneck, and R. W. Bigelow, J. Chem. Phys. 75, 4275 (1981).

93. D. A. Shirley, Phys. Rev. A9, 1549 (1974).

94. J. C. Fuggle and N. Martensson, J. Elect. Spectrosc. Related Phenom. 21, 275 (1980).

95. R. Hoogewijs, L. Fiermans, and J. Vennik, J. Elect. Spectrosc. Related Phenom. 11, 171 (1977).

96. G. Dufour, J. M. Mariot, P. E. N. Jatko, and R. C. Karnatak, Phys. Scr. 13, 370 (1976).

97 M. H. Chen and B. Crasemann, Phys. Rev. A8, 7 (1973).

98. C. D. Wagner, D. E. Passoja, H. F. Hillery, T. G. Kinisky, H. A. Six, W. T. Jansen, and J. A. Taylor, J. Vac. Sci. Technol. 21, 933 (1982).

FIGURES CAPTIONS

1. a) The derivative (d(EN(E))/dE) KVV Auger spectrum as obtained in this work. The estimated background is shown by the straight line.
   b) The integrated spectrum (solid Line), the loss spectrum (dot dashed line), and final deconvulited KVV lineshape (dashed line).

2. Plot of the s/p Auger atomic matrix elements ratios per filled s and p shells for the KL_1V, $KL_{23}V$, and $L_1L_{23}V$ processes. The s/p ratio for the $L_1L_{23}V$ process has been scaled by Z for Z < 24, by Z * 1.5 for Z > 24 as discussed in the text. The open circles indicate experimental data as tabulated by Babenkov et al. (27). The solid lines indicate the theoretical results from Chen et al (16), the dashed line theoretical results from Walters and Bhalla (30), the dotted and dot-dashed lines theoretical results from McGuire (31). The data points for Ar are discussed in the text (28, 29).

3. a) Comparison of the s DOS for Si as obtained from the Slater Koster parameterized tight binding Hamiltonian (14) and Gaussian broadened by 1.5 eV. (solid line) with that indicated from the $L_{23}V$ XES spectrum (dashed line) (41).
   b) Comparison of the core hole screened s DOS, as obtained from eq. (14) using the theoretical DOS above and a central potential of ϵ_s = 4. eV (solid line), with that indicated from the $L_{23}L_{23}$ - $L_{23}V$ XES (43) spectrum and the L_{23}

absorption spectrum (dashed line) (48a). The occupied theoretical DOS has been broadened by 5.5 eV. The unoccupied DOS has not been broadened.

4. a) Comparison of the theoretical p DOS obtained as in Fig. 3a (solid line) with that indicated by the KV XES spectrum (dashed line) (41).
   b) Comparison of the core hole screened p DOS, obtained as in Fig. 3b and using a valve of ϵ_p = 2. eV (solid line), with the K absorption spectrum (dashed line) (48b). The occupied DOS has been broadened by 3. eV, the unoccupied by 1.7 eV.

5. a) Comparison of the core hole screened s DOS for Si as obtained from eq. (14) utilizing the theoretical Slater Koster parameterized tight binding Hamiltonian and the central cell potentials of ϵ_s = 0, 2, 4, and 6 eV.
   b) Comparison of the core hole screened p DOS obtained as above.

6. Comparison of the experimental (variable dashed line) KL_1V lineshape (9) with the optimal fit of eq. (4) (solid line). The theoretical s and p contributions are indicated by the dashed lines. The experimental lineshape has been shifted by 2.04 eV to lower binding energy to provide an optimal fit with eq. (41).

7. Same as Fig. 6 but for the $KL_{23}V$ lineshape (9) which was shifted by 0.7 eV.

8. Same as Fig. 6 but for the $L_1L_{23}V$ lineshape (3) which was shifted by 0.4 eV.

9. Comparison of the experimental $L_{23}VV$ lineshape (3) with the optimal fit of eq. (5) and using $U = 0$ and 1.8 eV as described in the text. The theoretical sp and pp contributions are indicated by the dotted lines.

10. Comparison of the experimental KVV lineshape from Fig. 1 with the optimal fit of Eq. (5) and using $U_{ss} = 6$ eV , $U_{sp} = 4$ eV , and $U_{pp} = 2$ eV as described in the text. The resultant ss, sp and pp contributions are indicated by the dashed lines.

11. Comparison of the $KL_{23}L_{23}$ lineshape as obtained in this work (dashed) (Sec. 2) with that obtained by Cazaux and Minh Duc (22) (solid) using Bremsstrahlung radiation. A background has been substracted and losses deconvoluted as described in the text. The ^1D, ^1S, plasmon loss, and $KL-L^3$ shakeoff peaks are indicated.

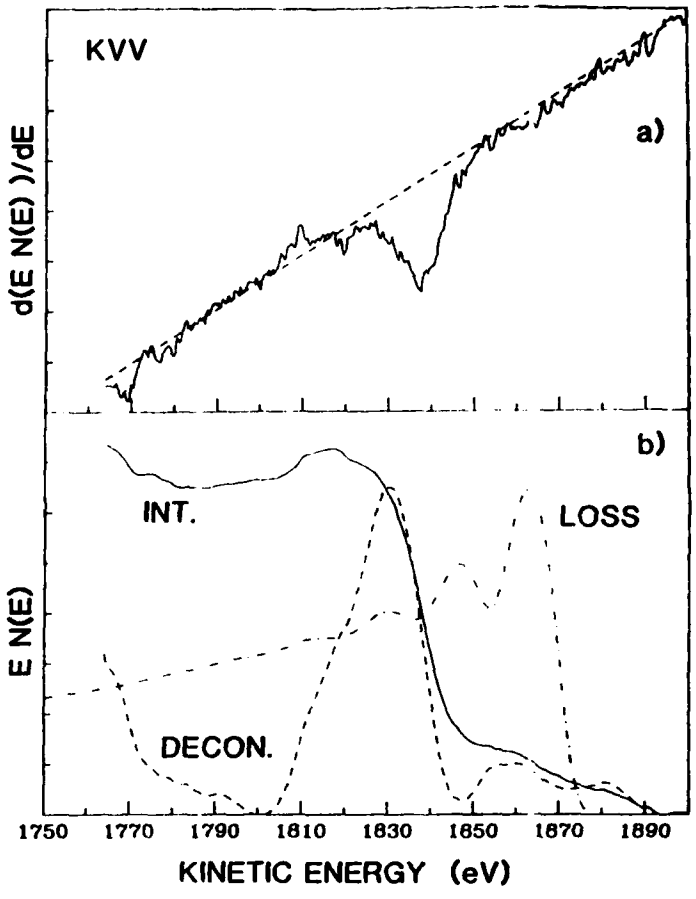

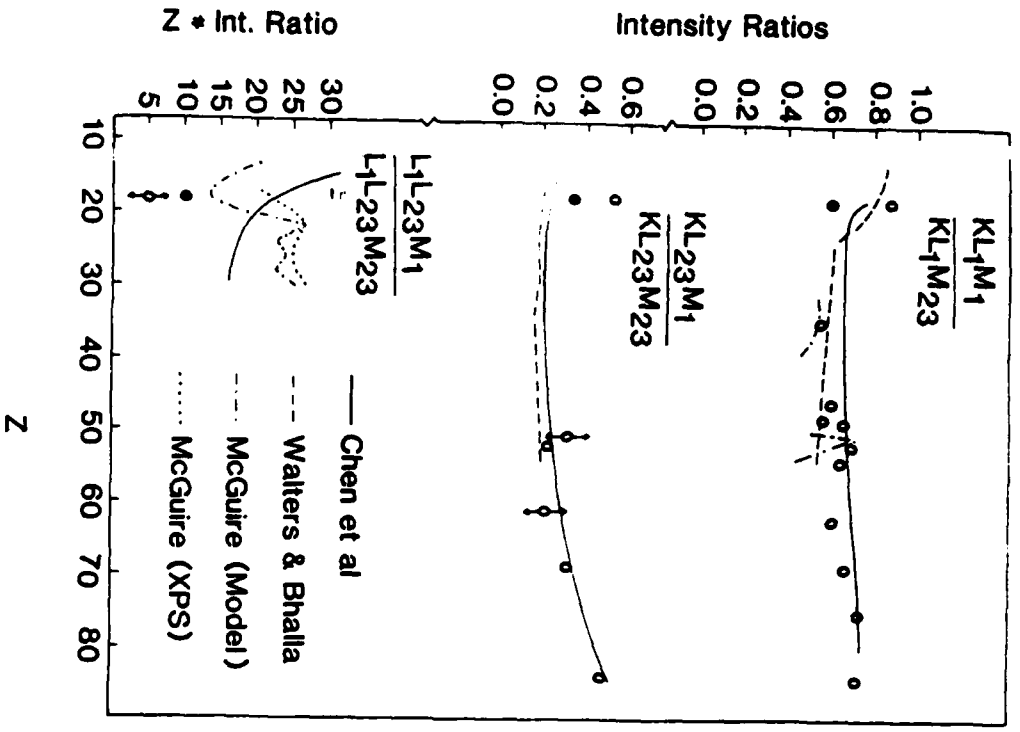
Z * Int. Ratio
Intensity Ratios
Z
KL_1M_1 / KL_1M_{23}
$KL_{23}M_1$ / $KL_{23}M_{23}$
$L_1L_{23}M_1$ / $L_1L_{23}M_{23}$
Chen et al
Walters & Bhalla
McGuire (Model)
McGuire (XPS)

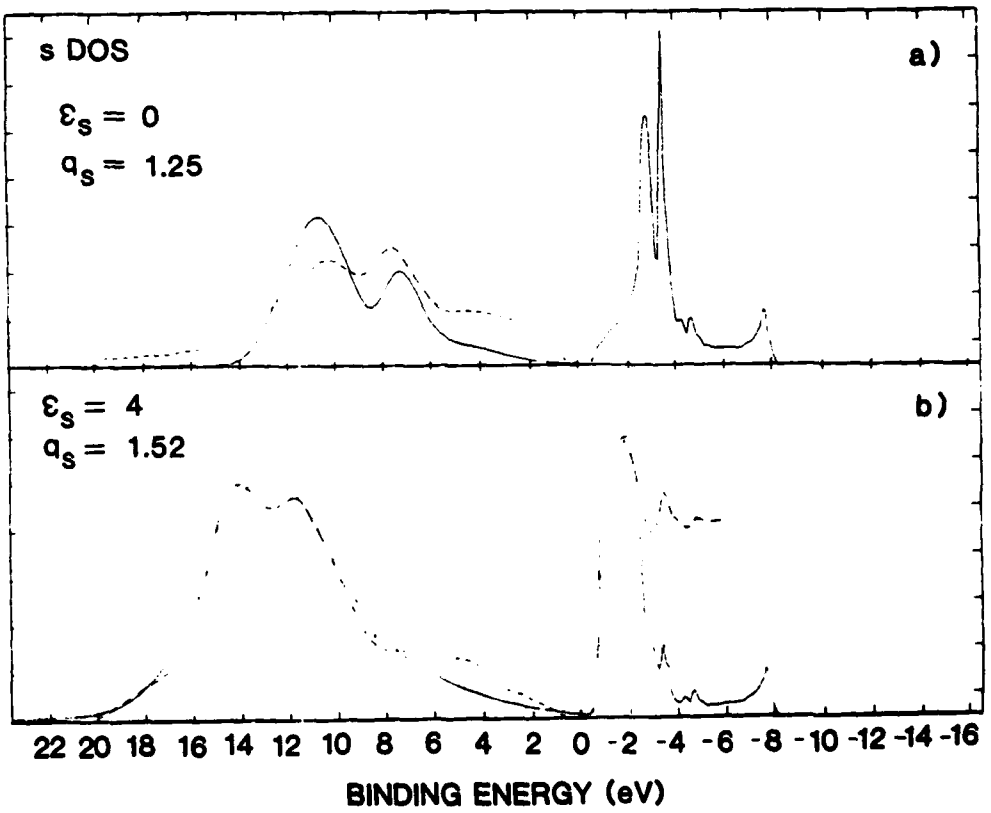
s DOS
a)
$\varepsilon_s = 0$
$q_s = 1.25$
$\varepsilon_s = 4$
b)
$q_s = 1.52$
22 20 18 16 14 12 10 8 6 4 2 0 -2 -4 -6 -8 -10 -12 -14 -16
BINDING ENERGY (eV)

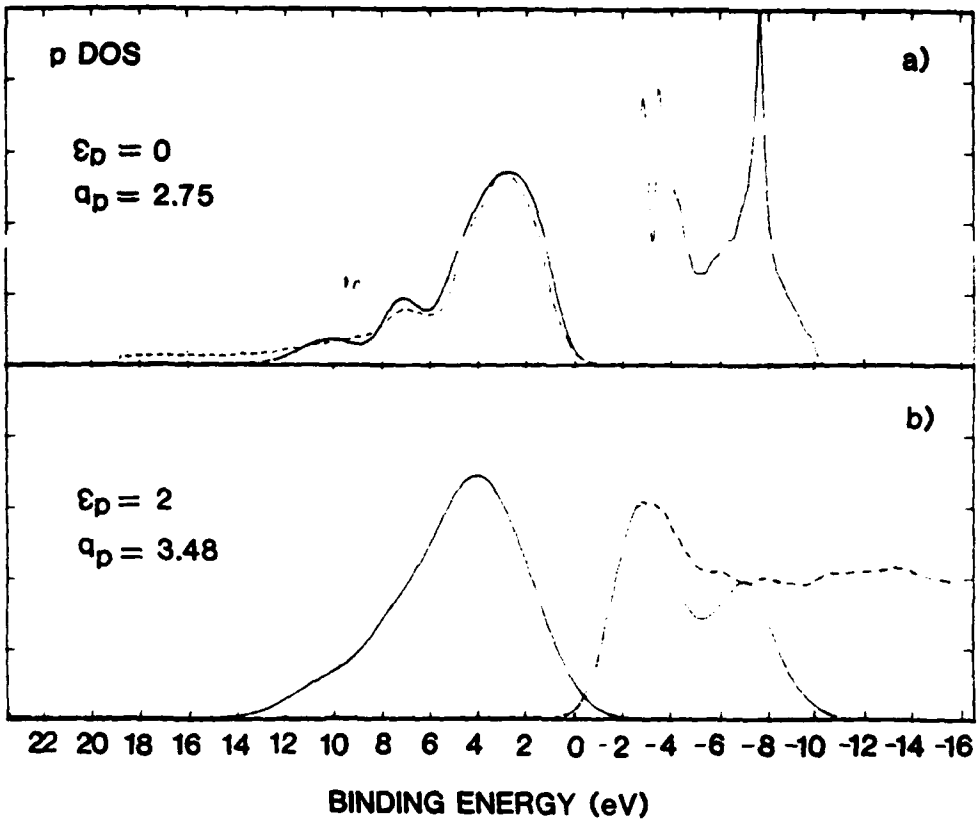
p DOS
a)
$\varepsilon_p = 0$
$q_p = 2.75$
b)
$\varepsilon_p = 2$
$q_p = 3.48$
22 20 18 16 14 12 10 8 6 4 2 0 -2 -4 -6 -8 -10 -12 -14 -16
BINDING ENERGY (eV)

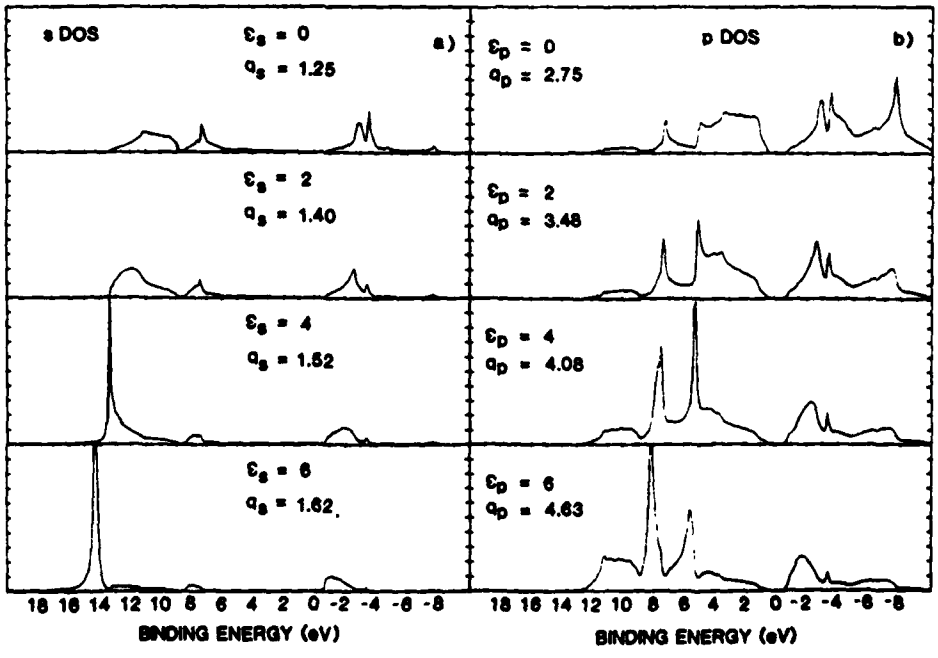
s DOS
$\varepsilon_s = 0$
$q_s = 1.25$
a)
$\varepsilon_s = 2$
$q_s = 1.40$
$\varepsilon_s = 4$
$q_s = 1.52$
$\varepsilon_s = 6$
$q_s = 1.62$
18 16 14 12 10 8 6 4 2 0 -2 -4 -6 -8
BINDING ENERGY (eV)
p DOS
$\varepsilon_p = 0$
$q_p = 2.75$
b)
$\varepsilon_p = 2$
$q_p = 3.48$
$\varepsilon_p = 4$
$q_p = 4.08$
$\varepsilon_p = 6$
$q_p = 4.63$
18 16 14 12 10 8 6 4 2 0 -2 -4 -6 -8
BINDING ENERGY (eV)

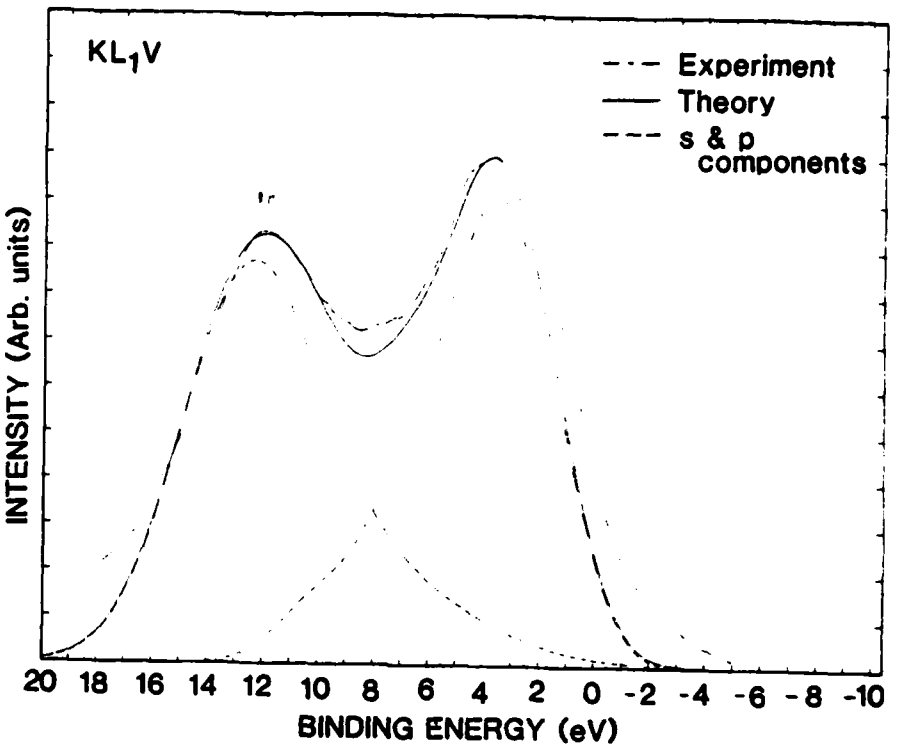
KL1V
Experiment
Theory
s & p components
INTENSITY (Arb. units)
20 18 16 14 12 10 8 6 4 2 0 -2 -4 -6 -8 -10
BINDING ENERGY (eV)

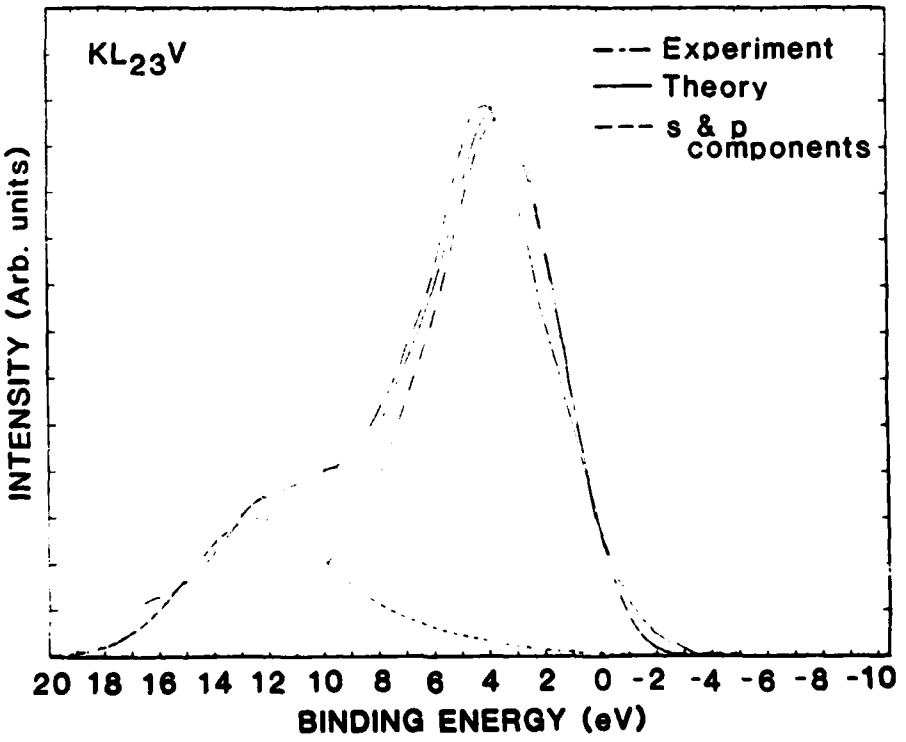
KL23V
Experiment
Theory
s & p components
INTENSITY (Arb. units)
20 18 16 14 12 10 8 6 4 2 0 -2 -4 -6 -8 -10
BINDING ENERGY (eV)

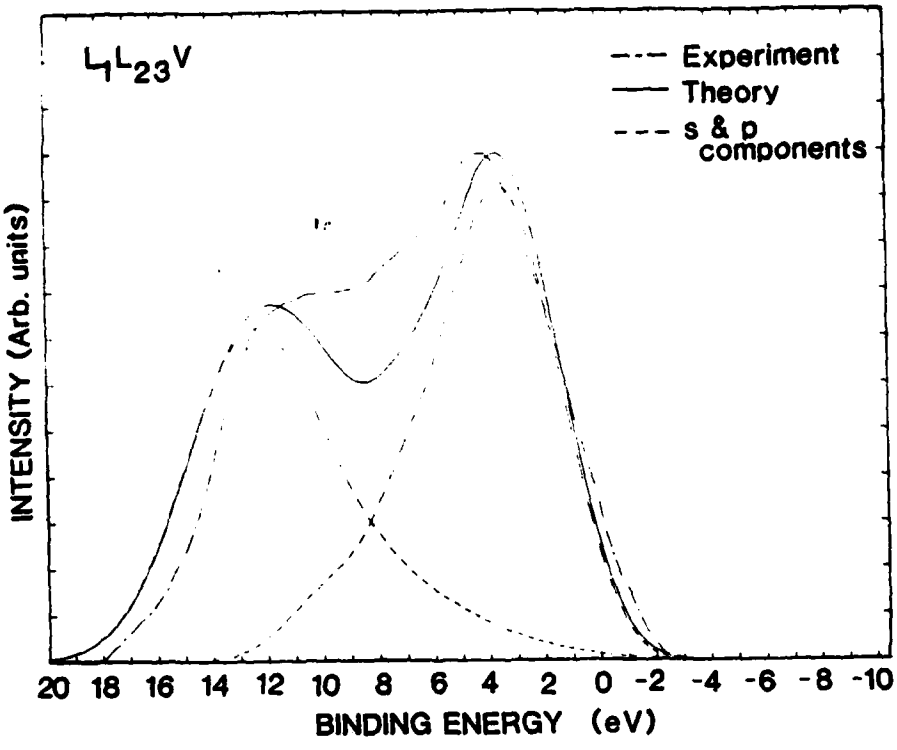
$L_1L_{23}V$
Experiment
Theory
s & p components
INTENSITY (Arb. units)
20 18 16 14 12 10 8 6 4 2 0 -2 -4 -6 -8 -10
BINDING ENERGY (eV)

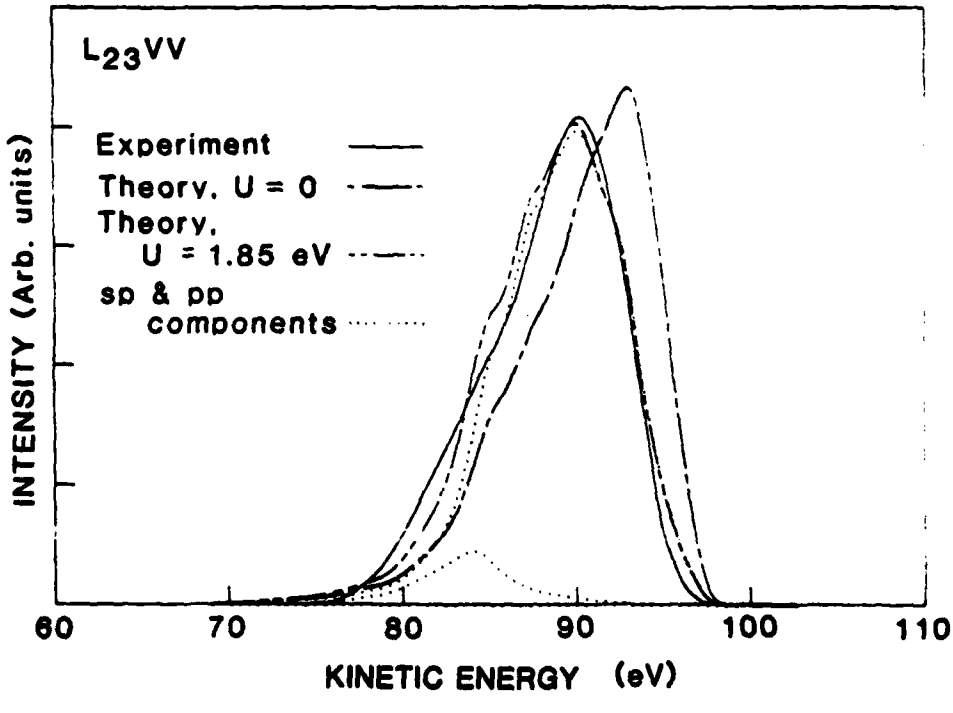
$L_{23}VV$
Experiment
Theory, U = 0
Theory, U = 1.85 eV
sp & pp components
INTENSITY (Arb. units)
60 70 80 90 100 110
KINETIC ENERGY (eV)

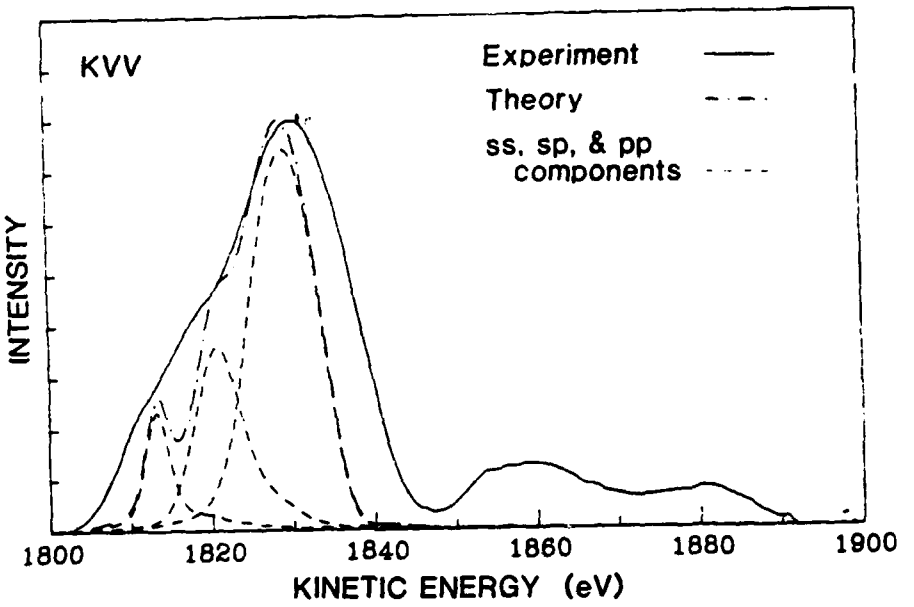
KVV
Experiment
Theory
ss, sp, & pp components
INTENSITY
1800
1820
1840
1860
1880
1900
KINETIC ENERGY (eV)

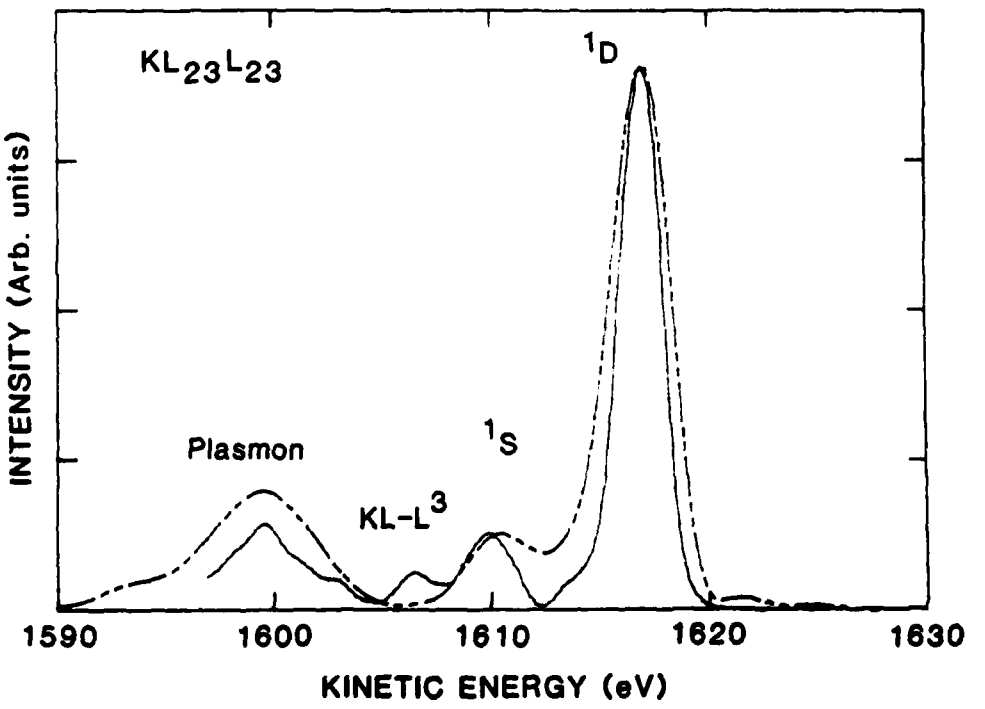
KL23L23
1D
1S
Plasmon
KL-L3
INTENSITY (Arb. units)
1590
1600
1610
1620
1630
KINETIC ENERGY (eV)

TECHNICAL REPORT DISTRIBUTION LIST, GEN

	No. Copies
Office of Naval Research Attn: Code 413 800 N. Quincy Street Arlington, Virginia 22217	2
Dr. Bernard Douda Naval Weapons Support Center Code 5042 Crane, Indiana 47522	1
Commander, Naval Air Systems Command Attn: Code 310C (H. Rosenwasser) Washington, D.C. 20360	1
Naval Civil Engineering Laboratory Attn: Dr. R. W. Drisko Port Hueneme, California 93401	1
Defense Technical Information Center Building 5, Cameron Station Alexandria, Virginia 22314	12
DTNSRDC Attn: Dr. G. Bosmajian Applied Chemistry Division Annapolis, Maryland 21401	1
Dr. William Tolles Superintendent Chemistry Division, Code 6100 Naval Research Laboratory Washington, D.C. 20375	1
Dr. David Young Code 334 NORDA NSTL, Mississippi 39529	1
Naval Weapons Center Attn: Dr. A. B. Amster Chemistry Division China Lake, California 93555	1
Scientific Advisor Commandant of the Marine Corps Code RD-1 Washington, D.C. 20380	1
U.S. Army Research Office Attn: CRD-AA-IP P.O. Box 12211 Research Triangle Park, NC 27709	1
Mr. John Boyle Materials Branch Naval Ship Engineering Center Philadelphia, Pennsylvania 19112	1
Naval Ocean Systems Center Attn: Dr. S. Yamamoto Marine Sciences Division San Diego, California 91232	1

ABSTRACTS DISTRIBUTION LIST, 056/625/629

Dr. G. A. Somorjai
Department of Chemistry
University of California
Berkeley, California 94720

Dr. J. Murday
Naval Research Laboratory
Surface Chemistry Division (6170)
455 Overlook Avenue, S.W.
Washington, D.C. 20375

Dr. J. B. Hudson
Materials Division
Rensselaer Polytechnic Institute
Troy, New York 12181

Dr. Theodore E. Madey
Surface Chemistry Section
Department of Commerce
National Bureau of Standards
Washington, D.C. 20234

Dr. J. E. Demuth
IBM Corporation
Thomas J. Watson Research Center
P.O. Box 218
Yorktown Heights, New York 10598

Dr. M. G. Lagally
Department of Metallurgical and Mining Engineering
University of Wisconsin
Madison, Wisconsin 53706

Dr. R. P. Van Duyne
Chemistry Department
Northwestern University
Evanston, Illinois 60637

Dr. J. M. White
Department of Chemistry
University of Texas
Austin, Texas 78712

Dr. D. E. Harrison
Department of Physics
Naval Postgraduate School
Monterey, California 93940

Dr. W. Kohn
Department of Physics
University of California, San Diego
La Jolla, California 92037

Dr. R. L. Park
Director, Center of Materials Research
University of Maryland
College Park, Maryland 20742

Dr. M. T. Peria
Electrical Engineering Department
University of Minnesota
Minneapolis, Minnesota 55455

Dr. Keith H. Johnson
Department of Metallurgy and Materials Science
Massachusetts Institute of Technology
Cambridge, Massachusetts 02139

Dr. S. Sibener
Department of Chemistry
James Franck Institute
5640 Ellis Avenue
Chicago, Illinois 60637

Dr. Arold Green
Quantum Surface Dynamics Branch
Code 3817
Naval Weapons Center
China Lake, California 93555

Dr. A. Wold
Department of Chemistry
Brown University
Providence, Rhode Island 02912

Dr. S. L. Bernasek
Department of Chemistry
Princeton University
Princeton, New Jersey 08544

Dr. P. Lund
Department of Chemistry
Howard University
Washington, D.C. 20059

ABSTRACTS DISTRIBUTION LIST, 056/625/629

Dr. F. Carter
Code 6132
Naval Research Laboratory
Washington, D.C. 20375

Dr. Richard Colton
Code 6112
Naval Research Laboratory
Washington, D.C. 20375

Dr. Dan Pierce
National Bureau of Standards
Optical Physics Division
Washington, D.C. 20234

Dr. R. Stanley Williams
Department of Chemistry
University of California
Los Angeles, California 90024

Dr. R. P. Messmer
Materials Characterization Lab.
General Electric Company
Schenectady, New York 22217

Dr. Robert Gomer
Department of Chemistry
James Franck Institute
5640 Ellis Avenue
Chicago, Illinois 60637

Dr. Ronald Lee
R301
Naval Surface Weapons Center
White Oak
Silver Spring, Maryland 20910

Dr. Paul Schoen
Code 5570
Naval Research Laboratory
Washington, D.C. 20375

Dr. John T. Yates
Department of Chemistry
University of Pittsburgh
Pittsburgh, Pennsylvania 15260

Dr. Richard Greene
Code 5230
Naval Research Laboratory
Washington, D.C. 20375

Dr. L. Kesmodel
Department of Physics
Indiana University
Bloomington, Indiana 47403

Dr. K. C. Janda
California Institute of Technology
Division of Chemistry and Chemical
Engineering
Pasadena, California 91125

Dr. E. A. Irene
Department of Chemistry
University of North Carolina
Chapel Hill, Northc Carolina 27514

Dr. Adam Heller
Bell Laboratories
Murray Hill, New Jersey 07974

Dr. Martin Fleischmann
Department of Chemistry
Southampton University
Southampton SO9 5NH
Hampshire, England

Dr. John W. Wilkins
Cornell University
Laboratory of Atomic and
Solid State Physics
Ithaca, New York 14853

Dr. Richard Smardzewski
Code 6130
Naval Research Laboratory
Washington, D.C. 20375

Dr. H. Tachikawa
Chemistry Department
Jackson State University
Jackson, Mississippi 39217

DL/413/83/01
056/413-2

ABSTRACTS DISTRIBUTION LIST, 056/625/629

Dr. R. G. Wallis
Department of Physics
University of California
Irvine, California 92664

Dr. D. Ramaker
Chemistry Department
George Washington University
Washington, D.C. 20052

Dr. J. C. Hemminger
Chemistry Department
University of California
Irvine, California 92717

Dr. T. F. George
Chemistry Department
University of Rochester
Rochester, New York 14627

Dr. G. Rubloff
IBM
Thomas J. Watson Research Center
P.O. Box 218
Yorktown Heights, New York 10598

Dr. Horia Metiu
Chemistry Department
University of California
Santa Barbara, California 93106

Captain Lee Myers
AFOSR/NC
Bollig AFB
Washington, D.C. 20332

Dr. J. T. Keiser
Department of Chemistry
University of Richmond
Richmond, Virginia 23173

Dr. Roald Hoffmann
Department of Chemistry
Cornell University
Ithaca, New York 14853

Dr. J. E. Jensen
Hughes Research Laboratory
3011 Malibu Canyon Road
Malibu, California 90265

Dr. J. H. Weaver
Department of Chemical Engineering
and Materials Science
University of Minnesota
Minneapolis, Minnesota 55455

Dr. R. W. Plummer
Department of Physics
University of Pennsylvania
Philadelphia, Pennsylvania 19104

Dr. E. Yeager
Department of Chemistry
Case Western Reserve University
Cleveland, Ohio 41106

Dr. N. Winograd
Department of Chemistry
Pennsylvania State University
University Park, Pennsylvania 16802

Dr. G. D. Stein
Mechanical Engineering Department
Northwestern University
Evanston, Illinois 60201

Dr. A. Steckl
Department of Electrical and
Systems Engineering
Rensselaer Polytechnic Institute
Troy, NewYork 12181

Dr. G. H. Morrison
Department of Chemistry
Cornell University
Ithaca, New York 14853

Dr. P. Hansma
Physics Department
University of California
Santa Barbara, California 93106

Dr. J. Baldeschwieler
California Institute of Technology
Division of Chemistry
Pasadena, California 91125

Dr. W. Goddard
California Institute of Technology
Division of Chemistry
Pasadena, California 91125

Dr. M. Knauer
Hughes Research Laboratory
3011 Malibu Canyon Road
Malibu, California 90265

Dr. C. B. Harris
Department of Chemistry
University of California
Berkeley, California 94720

END

FILMED

4-85

DTIC